https://doi.org/10.5194/hess-2022-400
Preprint. Discussion started: 13 December 2022

Hydrology and Earth System Sciences
Discussions

Stable water isotopes and tritium tracers tell the same tale: No evidence for underestimation of catchment transit times inferred by stable isotopes in SAS function models.

Siyuan Wang[1], Markus Hrachowitz[1], Gerrit Schoups[1], Christine Stumpp[2]

[1]Department of Water Management, Faculty of Civil Engineering and Geosciences, Delft University of Technology, Stevinweg 1, 2628CN Delft, Netherlands
[2]Institute of Soil Physics and Rural Water Management, University of Natural Resources and Life Sciences Vienna, Muthgasse 18, 1190 Vienna, Austria

Correspondence to: Siyuan Wang (S.Wang-9@tudelft.nl)

Abstract. Stable isotopes ($\delta^{18}O$) and tritium (^3H) are frequently used as tracers in environmental sciences to estimate age distributions of water. However, it has previously been argued that seasonally variable tracers, such as $\delta^{18}O$, generally and systematically fail to detect the tails of water age distributions and therefore substantially underestimate water ages as compared to radioactive tracers, such as ^3H. In this study for the Neckar river basin in central Europe and based on a >20-year record of hydrological, $\delta^{18}O$ and ^3H data, we systematically scrutinized the above postulate together with the potential role of spatial aggregation effects to exacerbate the underestimation of water ages. This was done by comparing water age distributions inferred from $\delta^{18}O$ and ^3H with a total of 12 different model implementations, including lumped parameter sine-wave (SW) and convolution integral models (CO) as well as integrated hydrological models in combination with SAS-functions (IM-SAS). We found that, indeed, water ages inferred from $\delta^{18}O$ with commonly used SW and CO models are with mean transit times (MTT) ~ 1 – 2 years substantially lower than those obtained from ^3H with the same models, reaching MTTs ~ 10 years. In contrast, several implementations of IM-SAS models did not only allow simultaneous representations of stream flow as well as $\delta^{18}O$ and ^3H stream signals, but water ages inferred from $\delta^{18}O$ with these models were with MTTs ~ 16 years much higher than those from SW and CO models and similar to those inferred from ^3H, which suggested MTTs ~ 15 years. Characterized by similar parameter posterior distributions, in particular for parameters that control water age, IM-SAS model implementations individually constrained with $\delta^{18}O$ or ^3H observations, exhibited only limited differences in the magnitudes of water ages in different parts of the models as well as in the temporal variability of TTDs in response to changing wetness conditions. This suggests that both tracers lead to comparable descriptions of how water is routed through the system. These findings provide evidence that allowed us to reject the hypothesis that $\delta^{18}O$ as a tracer generally and systematically "cannot see water older than about 4 years" and that it truncates the corresponding tails in water age distributions, leading to underestimations of water ages. Instead, our results provide evidence for a broad equivalence of $\delta^{18}O$ and ^3H as age tracers for systems characterized by MTTs of at least 15 – 20 years. The question to which degree aggregation of spatial heterogeneity can further adversely affect estimates of water ages remains unresolved as the lumped and distributed implementations of the

https://doi.org/10.5194/hess-2022-400
Preprint. Discussion started: 13 December 2022


Hydrology and Earth System Sciences
Discussions

IM-SAS model provided inconclusive results.

Overall, this study demonstrates that previously reported underestimations of water ages are most likely not a result of the use of $\delta^{18}O$ or other seasonally variable tracers per se. Rather, these underestimations can be largely attributed to choices of model approaches and complexity not considering hydrological next to tracer aspects. Given the additional vulnerability of SW and CO model approaches in combination with $\delta^{18}O$ to substantially underestimate water ages due to spatial aggregation and potentially other, still unknown effects, we therefore advocate to avoid the use of this model type in combination with seasonally variable tracers if possible, and to instead adopt SAS-based or comparable model formulations.

1 Introduction

Age distributions of water fluxes ("transit time distributions", TTD) and water stored in catchments ("residence time distributions", RTD) are fundamental descriptors of hydrological functioning (Botter et al., 2011; Sprenger et al., 2019) and catchment storage (Birkel et al., 2015). They provide a way to quantitatively describe the physical link between the hydrological response of catchments and physical transport processes of conservative solutes. While the former is largely controlled by the celerities of pressure waves propagating through the system, the latter, in contrast, occur at velocities that can be up to several orders of magnitude lower (McDonnell and Beven, 2014; Hrachowitz et al., 2016).

Water age distributions cannot be directly observed. Instead, they can, in principle, be inferred from observed tracer breakthrough curves. While practically feasible at lysimeter (e.g. Asadollahi et al., 2020; Benettin et al., 2021) and small hillslope scales (e.g. Kim et al., 2022), lack of adequate observation technology together with logistical constraints make this problematic at scales larger than that. At the catchment-scale, estimates of water age distributions are therefore typically inferred from models that describe the relationships between time-series of observed tracer input and output signals.

Over the past decades a wide spectrum of such models has been developed. Early approaches mostly relied on simple lumped sine-wave (hereafter: SW) or lumped parameter convolution integral models (hereafter CO; Maloszewski and Zuber, 1982,1983; McGuire and McDonnell, 2006), originally developed for aquifers. In spite of their wide-spread application, these models feature multiple critical simplifying assumptions. Most importantly, the vast majority of these model implementations work under the assumption that catchments are at steady state and that, as a consequence, TTDs are time-invariant and can be *a priori* defined or calibrated. While this assumption may have limited effect on TTDs in aquifers, given the temporal variability in the hydro-meteorological drivers of surface water systems (e.g. precipitation, atmospheric water demand) and the spatial heterogeneity in the hydrological processes, this assumption is violated in most environments world-wide and can lead to misinterpretations of the model results. This led to the development of a more coherent framework to estimate water age distributions without the need of an *a priori* definition of time-invariant TTDs. Instead, probability distributions, referred to as StorAge Selection (SAS) functions, are *a priori* defined or calibrated, and changes in water storage are considered. Thus, water fluxes within and released from the system are sampled from water volumes of different ages stored in the system according to these SAS functions (Botter et al., 2011; Rinaldo et al., 2015). The sampling procedure based on SAS functions

https://doi.org/10.5194/hess-2022-400
Preprint. Discussion started: 13 December 2022


Hydrology and Earth System Sciences
Discussions

thereby explicitly tracks the history of water (and tracer) input to and output from the system. As such it does account for non-steady state conditions, which in turn leads to the emergence of time-variable TTDs and RTDs (see review Benettin et al., 2022).

Irrespective of the modelling approach, two types of environmental tracers have in the past been frequently used to estimate water age distributions with the above models. The first type are tracers that are characterized by distinct differences in their seasonal signals. They include stable isotopes of water (^{2}H, ^{18}O; e.g. Maloszewski et al., 1983; Vitvar and Balderer, 1997; Fenicia et al., 2010) or solutes, such as Cl^- (e.g. Kirchner et al., 2001, 2010; Shaw et al., 2008; Hrachowitz et al., 2009a, 2015). With these tracers, water ages and (metrics of) their distributions can be estimated by the degree to which the seasonal amplitudes of the precipitation tracer concentrations are time-shifted and/or attenuated in the stream flow (McGuire and McDonnell, 2006; Kirchner, 2016). Broadly speaking, the stronger the attenuation of the seasonally variable tracer amplitude in stream flow (A_s) as compared to its amplitude in precipitation (A_p), i.e., the lower the amplitude ratio A_s/A_p, the older stream water is, on average. The second type of commonly used tracers are radioactive isotopes, such as tritium (^{3}H). Forming the basis for many water dating studies going back to the 1950s (e.g. Begemann and Libby, 1957; Eriksson, 1958; Dincer et al., 1970; Stewart et al., 2007; Morgenstern et al., 2010; Duvert et al., 2016; Gallart et al., 2016; Rank et al., 2018; Visser et al., 2019), water age can be estimated with radioactive tracers based on the level of radioactive decay experienced by precipitation input signals experience before they reach the stream.

The relationship between the tracer amplitude ratios A_s/A_p and water age that is exploited by seasonally variable tracers is highly non-linear. With increasing attenuation of the tracer signal in the stream, i.e., a lower A_s/A_p, water therefore does not only become older but the age estimates become more sensitive to changes in the amplitude ratio (Kirchner, 2016). This implies that the older the water, uncertainties in the observed amplitude ratios lead to increased uncertainties in water age estimates. As a consequence, there is an upper limit to the age of water which can be practically and feasibly practically and feasibly determined with seasonally variable tracers. A rare attempt to quantify this potential upper detectible age limit was reported by DeWalle et al. (1997). With an observed $\delta^{18}O$ precipitation amplitude A_p = 3.41‰, an assumed lowest possible $\delta^{18}O$ stream water amplitude that equaled the observational error A_s = 0.1‰, and the use of a lumped, time-invariant exponential TTD ("complete mixing") they determined a maximum detectable mean transit time (MTT) of around 5 years at their study site. Several authors subsequently emphasized that estimates of MTT and in particular of maximum detectable MTT such as reported by DeWalle et al. (1997) are specific to A_p at individual study sites (McGuire and McDonnell, 2006) and highly sensitive to choices in the modelling process (Stewart et al., 2010; Seeger and Weiler, 2014; Kirchner, 2016). For example, multiple previous studies demonstrated that the use of gamma distributions with a shape parameter $\alpha \sim 0.5$ as TTD produces model results that are more consistent with observed tracer data than the use of exponential distributions (i.e. $\alpha = 1$) in a wide range of contrasting environments world-wide (Kirchner et al., 2001; Godsey et al. 2010; Hrachowitz et al., 2010). Merely replacing the exponential distribution by a gamma distribution with $\alpha = 0.5$ as TTD at the study site of DeWalle et al. (1997) leads, in a quick back-of-the-envelope calculation, to a substantial increase of the maximum MTT from the reported 5 years to ~ 90 years. This is exacerbated by the potential presence of spatial aggregation bias in the lumped implementation

https://doi.org/10.5194/hess-2022-400
Preprint. Discussion started: 13 December 2022


Hydrology and Earth System Sciences
Discussions

of that model, which may cause further considerable underestimation of MTT as demonstrated by Kirchner (2016).

The relevance of the above assumptions is often overlooked and in spite of little additional quantitative evidence, it remains widely assumed that water ages in systems characterized by MTTs > 4 – 5 years cannot be meaningfully quantified with seasonally variable tracers. Most notably, Stewart et al. (2010, 2012) argued that water older than that remains *hidden* to stable water isotopes and other seasonally variable tracers, which inevitably results in a misleading truncation of water age distributions. Such a pronounced and systematic underestimation of water ages would have far reaching consequences for estimates of water storage (e.g. Birkel et al., 2015; Pfister et al., 2017) and the associated turnover times of nutrients and contaminants in catchments (e.g. Harman, 2015; Hrachowitz et al., 2015). Stewart et al. (2012), further argue that the use of radioactive tracers, such as ^{3}H, can largely avoid the truncation of the long tails of TTDs. This is mostly owed to the ^{3}H half-life of $T_{1/2}$ = 12.32 years. Even with the current atmospheric ^{3}H concentrations that, after peaking in the early 1960s, have been converging back towards pre-nuclear bomb testing levels, precipitation ^{3}H signals can be detected in the system for several decades, making ^{3}H an effective tracer now and for the foreseeable future (Michel et al., 2015; Harms et al., 2016; Stewart and Morgenstern, 2016). Indeed, a range of studies, based on ^{3}H and often in conjunction with lumped parameter convolution integral approaches, suggest that many catchments and larger river basins world-wide are characterized by MTTs that are decadal or higher (e.g. Stewart et al., 2010 and references therein). It is further rather remarkable that such elevated water ages are largely absent in estimates derived from lumped parameter convolution integral studies based on seasonally variable tracers, which often indicate MTTs between 1 – 3 years (e.g. McGuire and McDonnell, 2006 and references therein; Hrachowitz et al., 2009b; Godsey et al., 2010), as correctly and importantly pointed out by Stewart et al. (2010). This in itself could be supporting evidence for the failure of seasonally variable tracers to detect long tails of TTDs, as postulated by Stewart et al. (2012). However, it could just as well be a mere artifact arising from a sample bias due to the different catchments analyzed or from choices in the modelling process. There are only a few studies that have directly and systematically compared estimates of water age derived from both, seasonally variable (^{2}H, ^{18}O) and radioactive tracers (^{3}H) at the same study site and based on (at least partly) comparable model approaches (Maloszewski et al., 1983; Uhlenbrook et al., 2002; Stewart et al., 2007; Stewart and Thomas, 2008). The MTT estimates derived from seasonally variable tracers in these comparative studies are consistently, but to varying degrees lower than estimates based on ^{3}H. However, these studies are nevertheless subject to limitations that may weaken the generality of the conclusion that seasonally variable tracers underestimate catchment water ages. More specifically, tracer data were available for only rather short time periods of about 2 – 3 years, including, for some studies, only a handful of ^{3}H data points. All these studies relied on lumped parameter convolution integral approaches with time-invariant TTDs whose pre-defined functional form when applied with seasonally variable tracers was limited to shapes (e.g. exponential) that already *a priori* precluded the representation of long-tails and thus old ages. In addition, the models to estimate water ages in these studies were implemented in a spatially lumped way, which further exacerbates the potential for underestimating water ages due to spatial aggregation effects in environments that are likely subject to considerable heterogeneity in hydrological functioning (Kirchner, 2016).

Addressing some of the concerns above, a recent study by Rodriguez et al. (2021) compared catchment water ages inferred

https://doi.org/10.5194/hess-2022-400
Preprint. Discussion started: 13 December 2022


Hydrology and Earth System Sciences
Discussions

from two-year data records of a seasonally variable tracer (^{2}H; 1088 data points) and ^{3}H (24 data points) using a spatially lumped implementation of a previously developed simple tracer circulation model based on the SAS approach, which generates time-variable TTDs (Rodriguez and Klaus., 2019). In spite of consistently higher age estimates obtained from ^{3}H, the absolute differences to ^{2}H inferred estimates were very minor. While the difference in mean transit times was estimated at ΔMTT ~ 0.22 years for MTTs ~ 3 years, the difference in the estimate of the 90th percentile of water ages, as metric for the presence of old ages, was with Δ90th ~ 0.15 years even lower. The authors concluded that these results cast some doubt on "[…] the perception that stable isotopes systematically truncate the tails of TTDs" (Rodriguez et al., 2021). However, their interpretation was questioned by Stewart et al. (2021), who pointed out that simply no older water may be present in their study catchment.

Building on the above work of Rodriguez et al. (2021), the objective of this study is therefore to further scrutinize the notion that the use of seasonally variable tracers leads to truncated estimates of water age distributions in a systematic comparative experiment. The novel aspects of this study for the ~13.000 km^2 Neckar River basin in South-West Germany include that we here use (1) long-term records, i.e. > 20 years, of hydrological data as well as of seasonally variable (^{18}O) and radioactive tracers (^{3}H) together with (2) a spatially semi-distributed implementation of (3) an integrated, process-based model, making use of the SAS-function approach to simultaneously reproduce hydrological and tracer response dynamics and to track temporally variable water age distributions in the system and compare them to results using SW/CO models. The above points allow us to, at least partially, explore several unresolved questions how different factors may or may not contribute to the apparent underestimation of water ages by seasonally variable tracers, including potential effects of uncertainties arising from short data records, spatial aggregation and the use of oversimplified models. More specifically, we here test the hypothesis that ^{18}O as tracer generally and systematically cannot detect tails in water age distributions and that this truncation leads to systematically younger water age estimates than the use of ^{3}H.

2 Study site

The Neckar River basin in South-West Germany has an area of ~13,000 km^2. The elevation in the basin ranges from 122 m at the outlet in the north to about 1019 m in the South (Fig. 1a; Table 1). Following the elevation gradient, the landscape is characterized by terrace-like elements and undulating hills with wide valleys used as grass- and croplands in lower regions, in particular in the northern parts of the Neckar Basin, and increasingly steep and narrow forested valleys towards the southern parts (Fig. 1c). Long-term mean annual precipitation reaches ~909 mm yr^{-1}, with considerable spatial variability ranging from ~660 mm yr^{-1} in the lower parts of the basin to over 1500 mm yr^{-1} at high elevations in the southwest (Fig. 1b). With a long-term mean temperature of about 8.9 °C and an aridity index (i.e., $I_A = E_P/P$) I_A ~0.98 the basin is characterized by a temperate-humid climate, where snow cover can be present for several weeks in the winter months.

https://doi.org/10.5194/hess-2022-400
Preprint. Discussion started: 13 December 2022


Hydrology and Earth System Sciences
Discussions

3 Data

3.1 Data

Daily hydro-meteorological data were available for the period 01/01/1970 – 31/12/2016. As the forcing data of the hydrological models, daily precipitation and daily mean air temperature were obtained from stations operated by the German Weather Service (DWD). Precipitation was recorded at 16 stations and temperature measurements were available at 12 stations (Fig. 1) in or close to the study basin. Daily mean discharge data for the period 01/01/1970 – 31/12/2016 at the outlet of the Neckar basin at Rockenau station were provided by the German Federal Institute of Hydrology (BfG).

Long-term volume-weighted monthly $\delta^{18}O$ data in precipitation was available for the period 01/01/1978 – 31/12/2016 at the Stuttgart station. At the sampling gauge, a monthly accumulation bottle was filled with the collected daily precipitation, and all collected water was mixed together. Therefore, the water samples of precipitation reflect the volume-weighted monthly isotopic composition. Then, a monthly isotope sample bottle for stable isotope (i.e., ^{18}O) was filled with 50 ml precipitation water from the corresponding monthly accumulation bottle. All precipitation samples were tightly sealed and stored in a dark room at ~4°C before analysis. Monthly stream water samples were collected at Schwabenheim, close to the Rockenau discharge station, by the BfG for the period of 01/10/2001 – 31/12/2016 (Schmidt et al. 2020; Königer et al. 2022). Note that the available data do not represent instantaneous grab samples but bulk samples from mixed daily samples. River water was sampled automatically by samplers (SP III-XY-36, Maxx Meb- und Probenahmetechnik GmbH, Germany), which contained 36 bottles (each with a volume of 2.5 L). Every 30 minutes, 50 ml river water was pumped into one bottle (48 subsamples per day). A new bottle was filled every 24 h with the same procedure. All daily river water samples were stored in the sample compartment at ~4°C and were subsequently combined into monthly samples in the laboratory of BfG. This means the stream water samples reflect a non-flow-weighted monthly average isotopic composition. The stable isotopes ratios were analyzed with dual-inlet mass spectrometry and a laser-based cavity ring-down spectrometer (L2120-i/L2130-i, Picarro Inc.) at Helmholtz Zentrum München, Germany. When changing from dual-inlet mass spectrometry to cavity ring-down spectrometry, the long-term precision of the analytical systems (±0.15 ‰ and ±0.1 ‰, respectively, for $\delta^{18}O$) was ensured (Stumpp et al. 2014; Reckerth et al., 2017).

Long-term monthly ^{3}H data in precipitation were obtained for the period 01/01/1978 – 31/12/2016 at Stuttgart station (same station as ^{18}O data in precipitation; Schmidt et al., 2020). For the purpose of establishing robust initial conditions for the model experiment (see section 4.2) the tritium record in precipitation was reconstructed for the preceding 1970-1977 period by bias correcting data from the sampling station Vienna, available from the Global Network of Isotopes in Precipitation which is a joint database of the International Atomic Energy Agency (IAEA) and the World Metrological Organization (WMO) (Supplementary Material Fig. S1). The precipitation for tritium data was sampled based on the same method as that for ^{18}O in precipitation which means that the precipitation samples for tritium also reflect the volume-weighted monthly isotopic composition. Stream water samples for tritium were collected based on the same method as that for as ^{18}O in stream. Therefore, tritium stream water samples also reflect non-volume-weighted monthly average isotopic compositions. All water samples

https://doi.org/10.5194/hess-2022-400
Preprint. Discussion started: 13 December 2022


Hydrology and Earth System Sciences
Discussions

195 were analyzed for tritium concentrations by the BfG Environmental Radioactivity Laboratory using liquid scintillation counters (Ultima Gold LLT) with a 2-sigma analytical uncertainty (Schmidt et al. 2020).

Land use types of the catchments are determined using the CORINE Land Cover data set of 2018 (https://land.copernicus.eu/pan-european/corine-land-cover). The 90 m × 90 m digital elevation model of the study region (Fig. 1a) was obtained from https://www.usgs.gov/ and used to derive the local topographic indices including height above nearest
200 drainage (HAND) and slope.

3.2 Data pre-processing

For the subsequent model experiment (section 4.2), the study basin was stratified into four regions P1 – P4 that are characterized by distinct long-term precipitation pattern (hereafter: precipitation zones). In the following the procedure to infer these precipitation zones and to estimate the associated differences in $\delta^{18}O$ and ^{3}H input is described.

205 3.2.1 Spatial distribution of precipitation and identification of precipitation zones

To account, at least to some degree, for spatial heterogeneity in precipitation we stratified the Neckar River basin into precipitation zones that are each characterized by distinct average annual precipitation totals. Goovaerts (2000) and Lloyd (2005) showed that areal precipitation estimates informed by elevation data were often more accurate than those based on precipitation gauge observations alone. Thus, to interpolate and to estimate areal precipitation across the basin we used Co-
210 Kriging, considering elevation, as a preliminary analysis suggested lower errors. Finally, the individual precipitation estimates for each grid cell were used with K-means clustering to establish four clusters, representing the four precipitation zones P1 – P4 (see Fig. 1b).

3.2.2 Spatial extrapolation of precipitation $\delta^{18}O$ to precipitation zones

Records of observed precipitation $\delta^{18}O$ are available at one location close to the center of the Neckar Basin (Fig. 1). However,
215 it is well described (e.g. Kendall and Mcdonnell, 2012) that precipitation $\delta^{18}O$ input can be subject to considerable spatial heterogeneity, largely controlled by topographic and meteorological influences. Stumpp et al. (2014) specifically identified latitude, elevation and temperature as the key factors controlling $\delta^{18}O$ input heterogeneity in the greater study region. To at least partially account for these effects and to locally adjust $\delta^{18}O$ input signals throughout the study basin, we made use of the sinusoidal isoscapes method (Allen et al., 2018, 2019). Briefly, this method exploits the seasonal pattern in $\delta^{18}O$ precipitation
220 signal by fitting sine functions to observed $\delta^{18}O$ input signals for a large sample of locations:

$$\delta^{18}O_P(t) = a_P \sin(2\pi t - \varphi_P) + b_P, \quad (1)$$

With a_P [‰] the amplitude of the seasonal precipitation signal, b_P [‰] a constant offset and φ_P [rad] the phase of the signal. For each of the three fitting parameters, i.e., a_P, b_P and φ_P, multiple regression relationships were previously developed (Allen et al., 2018). Depending on the fitting parameter, predictor variables included a selection of latitude, longitude, elevation, range

https://doi.org/10.5194/hess-2022-400
Preprint. Discussion started: 13 December 2022


Hydrology and Earth System Sciences
Discussions

of annual temperature range and mean annual precipitation (Allen et al., 2018). The relationships defined by these predictor variables then allow to estimate a_P, b_P and φ_P, and thus the seasonal signal of $\delta^{18}O_P$ for locations where no precipitation $\delta^{18}O$ observations are available.

Here, we adopted the method as described in the following. In a first step, we estimated the sine wave parameters for the time series of precipitation $\delta^{18}O$ observed at the station Stuttgart, using the procedure described by Allen et al. (2018). Subsequently, we estimated the associated sine wave parameters a_P, b_P and φ_P in each of the four precipitation zones (P1 – P4; Supplementary Material Table S2) based on Eqs. (S1) - (S3) in the Supplement, using the above-described individual predictor variables, averaged for each precipitation zone (Supplementary Material Table S1). We then used the estimated sine wave parameters to construct an individual $\delta^{18}O_P$ sine wave for each precipitation zone (Eq.1). In a last step, we adjusted the observed $\delta^{18}O$ input for the four precipitation zones by rescaling and bias correcting the observed $\delta^{18}O$ signal according to the differences between the sine waves at the observation station and sine waves estimated for each precipitation zone, respectively (Supplementary Material Fig. S2).

3.2.3 Spatial extrapolation of precipitation ^3H to precipitation zones

As for $\delta^{18}O$, it is well documented that ^3H exhibits spatial heterogeneity that is to some extent controlled by geographical factors. It has been shown that the ^3H concentration in precipitation increases with latitude, with highest concentrations in polar regions (Rozanski et al., 1991). In addition, ^3H concentrations in precipitation increase with elevation due to the ^3H-enriched upper troposphere and isotopic exchange between liquid water and atmospheric moisture, depleting ^3H in lower tropospheric layers (Tadros et al., 2014). Considering the above effects, we established a multiple linear regression relationship between ^3H concentrations in precipitation observed at 15 multiple locations across Germany (Supplementary Material Fig. S3) as available through the WISER database (IAEA and WMO, 2022; Schmidt et al., 2020), and their corresponding elevation and latitude, respectively (Supplementary Material Fig. S4). We then used this relationship to adjust the ^3H precipitation input for the four precipitation zones according to their corresponding average latitude and elevation estimate:

$$^3H_P(t) = -0.75(L_P - L_o) - 0.002(E_P - E_o) + {}^3H_o, \quad (2)$$

where ^3H_P is the latitude- and elevation-adjusted tritium precipitation concentration for each precipitation zone (P1 – P4), ^3H_o is the tritium precipitation concentration observed at the Stuttgart station, L_P and E_P are the mean latitude and elevation, respectively, of each precipitation zone and L_o and E_o are the latitude and elevation, respectively, of the Stuttgart station.

4 Methods

The experiment to test the hypothesis that the use of $\delta^{18}O$ data systematically leads to truncated water age distributions and associated underestimations of water ages is designed and executed in a step-wise approach. Twelve different model types and spatial implementations thereof are sequentially calibrated (and tested) to reproduce observed $\delta^{18}O$ and ^3H signals in stream

https://doi.org/10.5194/hess-2022-400
Preprint. Discussion started: 13 December 2022


Hydrology and Earth System Sciences
Discussions

flow. For these models, several metrics of water age distributions resulting from the 2 independent calibration procedures, i.e., for $\delta^{18}O$ and ^{3}H, respectively, are then estimated and compared. As a baseline and to ensure comparability with previous studies, water ages are quantified with spatially lumped implementations of 9 model scenarios (Table 2): sine-wave models using exponential (SW-EM) and gamma distributions as TTDs (SW-GM; only $\delta^{18}O$), lumped parameter convolution integral models using exponential (CO-EM) and gamma distributions as TTDs (CO-GM) and a spatially integrated hydrological model with tracer routing based on SAS-functions (IM-SAS-L). Estimates of water ages from these spatially lumped model implementations are then compared to water ages inferred from 3 spatially distributed implementations of the same integrated hydrological model in combination with SAS-functions (IM-SAS-D).

4.1 Models

4.1.1 Sine-wave model (SW)

As demonstrated by Małoszewski et al. (1983), sine waves fitted to $\delta^{18}O$ precipitation and stream flow signals can be used to indicatively determine water ages. More specifically, the ratio of the amplitudes of the fitted sine waves, i.e. A_s/A_p, can be used together with the assumption of a shape of the TTD to estimate the associated MTT of a system. In the case of a gamma distribution as TTD, this is done according to (Kirchner, 2016):

$$\bar{\tau} = \alpha\beta, \tag{3}$$

with

$$\beta = \frac{1}{2\pi f}\sqrt{\left(A_s/A_p\right)^{-2/\alpha} - 1}, \tag{4}$$

where $\bar{\tau}$ is the MTT, α is a shape parameter, β is a scale parameter and f here is the frequency for the seasonal $\delta^{18}O$ signal, i.e., f = 1 yr^{-1}. Here we analyze the two cases α =1 (SW-EM) and 0.5 (SW-GM). Note that with α = 1, the gamma distribution is equivalent to an exponential distribution. The sine wave model is a simplification of a convolution integral model and can be directly derived from that. For a more detailed description of the method and underlying assumptions we refer to McGuire and McDonnell (2006) and Kirchner (2016).

4.1.2 Lumped parameter convolution integral model (CO)

While the sine wave approach requires regular cyclic signals of tracer composition, i.e., sine waves fitted to the observations, convolution integral models make direct use of the observed tracer data (e.g. Kreft and Zuber, 1978). Tracer composition in the system output can thus be estimated based on a convolution operation of the tracer composition in the system input together with an *a priori* assumption of a TTD (e.g. Maloszewski and Zuber, 1982):

$$C_o(t) = \int_0^\infty g(\tau)C_i(t-\tau)e^{-\lambda\tau}\,d\tau, \tag{5}$$

https://doi.org/10.5194/hess-2022-400
Preprint. Discussion started: 13 December 2022


Hydrology and Earth System Sciences
Discussions

Where $C_o(t)$ is the tracer composition of the system output (here: stream flow) at time t, $C_i(t-\tau)$ is the tracer composition of the system input (here: precipitation) at any previous time $t-\tau$, λ is the radioactive decay constant ($\lambda = 0.00015$ d^{-1} for ^{3}H and $\lambda = 0$ d^{-1} for stable isotopes) and $g(\tau)$ is the distribution of transit times τ. Here, we used gamma distributions as TTDs (e.g. Kirchner et al., 2001):

$$g(\tau) = \frac{\tau^{\alpha-1}}{\beta^{\alpha}\Gamma(\alpha)} e^{\frac{-\tau}{\beta}}, \quad (6)$$

With the shape parameter α and the scale parameter β being calibration parameters. The MTT associated with these parameters is then obtained with Eq. (3). Here we use the two cases $\alpha = 1$ (CO-EM) and 0.5 (CO-GM) for both, $\delta^{18}O$ and ^{3}H, to estimate the respective MTTs, and only β is treated as a free calibration parameter. For more detailed description of the method, refer to McGuire and McDonnell (2006).

4.1.3 Integrated model (IM-SAS)

A previously developed process-based model, based on the DYNAMITE modular modelling scheme (Hrachowitz et al., 2013, 2021), was iteratively customized and tested for the Neckar study basin. To allow for simultaneous representation of water and tracer fluxes, the hydrological model was adapted with additional, hydrologically passive water storages volumes from which water and tracer fluxes were sampled using the storage-age selection function (SAS) concept as outlined by Rinaldo et al. (2015). Water ages, their distributions, and the associated moments thereof were then estimated by tracking water and tracer fluxes through the model.

Hydrological model
The hydrological model consists of a suite of storage components and associated water fluxes between them. The influence of functionally different landscape elements, i.e. forest, grass-/cropland and flat valley bottoms, for brevity hereafter referred to as wetland, is represented by parallel hydrological response units (HRU), linked by a common storage component representing the groundwater system (Fig. 2), as previously implemented and successfully tested in many contrasting environments (e.g. Gao et al., 2014; Gharari et al., 2014; Euser et al., 2015; Nijzink et al., 2016; Prenner et al., 2018; Hanus et al., 2021). Briefly, precipitation P (mm d^{-1}) falling on days with temperatures below threshold temperature T_t (°C), is accumulated as snow P_{snow} (mm d^{-1}) in the snow storage S_{snow} (mm). On days with temperatures higher than that, precipitation enters the system as rainfall P_{rain} (mm d^{-1}) and, based on a simple degree-day approach, water is released from S_{snow} as snow melt M_{snow} (mm d^{-1}), controlled by melt factor C_{melt} (mm d^{-1} °C^{-1}; e.g. Gao et al., 2017; Girons Lopez et al., 2020). Rain water is then routed through the interception storage S_i (mm). With E_i (mm d^{-1}) as interception evaporation at the potential evaporation rate, effective precipitation P_{re} (mm d^{-1}) generated by overflow once the maximum interception capacity (S_{imax}) is exceeded, together with M_{snow}, enters the unsaturated root-zone S_u (mm). From S_u water can then be released as vapor via a combined soil evaporation and transpiration flux E_a (mm d^{-1}). Drainage of liquid water from S_u can either recharge the groundwater S_s (mm) over a

https://doi.org/10.5194/hess-2022-400
Preprint. Discussion started: 13 December 2022


Hydrology and Earth System Sciences
Discussions

percolation flux R_{perc} (mm d^{-1}) and a faster preferential recharge R_{pref} (mm d^{-1}). Alternatively, it can be routed via R_{uf} (mm d^{-1}) to a faster responding component S_f (mm) from where it is directly released to the stream as Q_f (mm d^{-1}), representing lateral preferential flow. Rain and snow melt entering the wetland HRU directly reach S_u. Soil moisture levels in the wetland S_u are further sustained by a fraction of groundwater R_{cap} (mm d^{-1}) that is upwelling into S_u from S_s (e.g., Hulsman et al., 2021a). The detailed equations of the model are provided as Table S3 in the Supplementary Material.

Tracer transport model

$\delta^{18}O$ and ^3H were routed through the above-described storage components (Fig.2) by sampling the modeled outflow volumes that leave the individual components at each time step t (d) (e.g. M_{snow}, R_{perc}, E_a, etc.) from the individual water volumes of different age T (d) that are stored in the associated storage component (e.g. S_{snow}, S_u, etc.) at each time step according to a SAS function. The distribution of water volumes of different ages in each storage component, i.e., the residence time distribution RTD, depends on the past sequence of inflows I (mm d^{-1}) and outflows O (mm d^{-1}) and therefore varies over time. As a consequence of being sampled from RTDs that evolve over time, both, inflows I and outflows O are correspondingly characterized by water age distributions (or transit time distributions TTD) that change over time. A straightforward implementation of this SAS concept is facilitated by the formulation of age-ranked storages $S_T(T,t)$ (mm). As emphasized by Benettin et al. (2017), $S_T(T,t)$ describes "at any time t the cumulative volumes of water in a storage component as ranked by their age T". Correspondingly, the total inflow (I) into as well as the total outflow volumes (O) from different storages can be expressed in terms of their cumulative, age-ranked volumes $I_T(T,t)$ and $O_T(T,t)$ (mm d^{-1}). At any time, closing the resulting water age balance for each storage component j (e.g. S_{snow}, S_u, etc.) also leads to an updated age-ranked storage $S_{T,j}(T,t)$ for that component, formulated as (Benettin et al., 2015a; Botter et al., 2011; Harman, 2015; Van Der Velde et al., 2012):

$$\frac{\partial S_{T,j}(T,t)}{\partial t} + \frac{\partial S_{T,j}(T,t)}{\partial T} = \sum_{n=1}^{N} I_{T,n,j}(T,t) - \sum_{m=1}^{M} O_{T,m,j}(T,t), \quad (7)$$

Where $\partial S_T/\partial T$ is the aging process of water in storage. Here, the water age balance (Eq.7) was formulated individually for each storage reservoir j, also accounting for different numbers N of storage component inflows I (e.g. P_{rain}, M_{snow}, R_{perc}) and numbers M of outflows O (e.g., R_{perc}, R_{pref}, E_a) (Fig. 2), similar to previous studies (e.g. Hrachowitz et al., 2021). For a daily modelling time step, it can in the water age balance be assumed that precipitation P(t) that is falling on day t is characterized by an age T = 0. This implies for the age ranked inflow $I_{T,P,j}(0,t) = P_T(0,t) = P(t)$. Note, that all other age ranked inflows $I_{T,n,j}(T,t)$ that enter a storage component are equivalent to the corresponding age ranked outflows $O_{T,m,j}(T,t)$ that leave a "higher" storage component.

Depending on the total volume of outflow $O_{m,j}(t)$ and the cumulative distribution of ages $P_{o,m,j}(T,t)$ of that flow, an age-ranked outflow $O_{T,m,j}(T,t)$ for each flux m released from each storage component j can be defined as:

$$O_{T,m,j}(T,t) = O_{m,j}(t) P_{o,m,j}(T,t), \quad (8)$$

While the outflow $O_{m,j}(t)$ from any storage component j is computed for each time step t by the hydrological model described

https://doi.org/10.5194/hess-2022-400
Preprint. Discussion started: 13 December 2022

above, the associated $P_{o,m,j}(T,t)$ cannot be assumed to be known as it is controlled by the temporally evolving distribution of water ages present in that storage component $S_{T,j}(T,t)$ at t. However, the temporally variable $P_{o,m,j}(T,t)$ can be inferred for each time step t by defining for each storage j and for each outflow m released from j a SAS function $\omega_{o,m,j}$ together with its cumulative form $\Omega_{o,m,j}$. These functions then describe how the water volumes of different ages, stored in component j at time t, i.e. $S_{T,j}(T,t)$, are sampled and combined into the corresponding total outflow volume $O_{m,j}(t)$:

$$P_{o,m,j}(T,t) = \Omega_{o,m,j}\big(S_{T,j}(T,t),t\big), \tag{9}$$

The probability density function $p_{o,m,j}(T,t)$ associated with the cumulative distribution of ages $P_{o,m,j}(T,t)$, then represents the transit time distribution TTD of that outflow and can be written as:

$$p_{o,m,j}(T,t) = \varpi_{o,m,j}\big(S_{T,j}(T,t),t\big)\frac{\partial S_{T,j}}{\partial T}, \tag{10}$$

Conservation of mass dictates that

$$\Omega_{o,m,j}\big(S_{T,j}(T,t) \to S_j(t),t\big) = 1, \tag{11}$$

Where S_j (mm) is the total volume of water stored in component j at time t. The resulting need to rescale $\omega_{o,m,j}$ for each time step was here avoided by instead normalizing and therefore bounding the age ranked storage to the interval [0,1] according to

$$S_{T,norm,j}(T,t) = \frac{S_{T,j}(T,t)}{S_j(t)}, \tag{12}$$

Note that $S_{T,norm,j}$ also represents the RTD of storage component j at time t.

In this study, we used uniform distributions in the form of ω = const. as SAS function in each storage component as previously shown to be effective in many studies (e.g. Birkel et al., 2011; van der Velde et al., 2015; Benettin et al., 2015b, 2017; Ala-Aho et al., 2017; Kuppel et al., 2018; Rodriguez et al., 2018). This implies random sampling and the assumption that each storage component is fully mixed and that there is no preference for sampling younger or older water. Here, it is important to note that the "combined" SAS functions of all storage components will, due to distinct storage capacities and time-scales, *not* lead to an overall system response that is fully mixed. Uniform SAS functions were here chosen over other shapes, such as beta-distributions (e.g. van der Velde et al., 2012; Hrachowitz et al., 2021), as they do not need additional model parameters and avoid the need for explicit calculation of TTDs at each model time step to route tracers through the model (Benettin et al., 2015b), thereby drastically reducing computational time and computer memory requirements (Benettin et al., 2022).

To adequately damp tracer input signals, additional and hydrologically passive storage volumes are typically required (e.g. Birkel et al., 2010; Hrachowitz et al., 2015, 2016). Such a passive water storage volume $S_{s,p}$ (mm), characterized by $d_{Ss,p}/dt = 0$, was added as calibration parameter to the active groundwater storage Ss (Fig. 2). While the outflow Q_s from the groundwater storage is exclusively regulated by the temporally varying storage volume in S_s (Supplementary Material Eq. S9), the tracer and age composition of that outflow is sampled from the total groundwater storage volume $S_{s,tot} = S_s + S_{s,p}$.

https://doi.org/10.5194/hess-2022-400
Preprint. Discussion started: 13 December 2022


Hydrology and Earth System Sciences
Discussions

The $\delta^{18}O$ and ^{3}H concentrations were then routed through each individual storage component according to (e.g. Harman, 2015; Benettin et al., 2017):

$$C_{o,m,j}(t) = \int_0^{S_j} C_{s,j}\left(S_{T,j}(T,t),t\right)\omega_{o,m,j}\left(S_{T,j}(T,t),t\right)e^{-\lambda T}\, dS_T, \quad (13)$$

Where $C_{o,m,j}$ is the tracer concentration in outflow m from storage component j at time t, $C_{s,j}$ is the tracer concentration of water in storage at time t and λ is the radioactive decay constant (λ = 0 d^{-1} for $\delta^{18}O$ and λ = 0.00015 d^{-1} for ^{3}H).

4.2 Model implementation

4.2.1 Spatially lumped model implementation

The original argument that the use of seasonally variable tracers underestimates water ages was exclusively based on lumped implementations of sine-wave and convolution integral models (Stewart et al., 2010). For a baseline comparison and to check whether the above conclusion would also have been reached for our study basin using the same methods, we here similarly implemented the sine-wave (SW-EM, SW-GM) and convolution integral (CO-EM, CO-GM) in a spatially lumped way. For this baseline case the catchment average tracer input was estimated as the spatially weighted mean from the four precipitation zones P1 – P4 as described in section 3.2.

The spatially lumped implementation of the integrated model (IM-SAS-L) was also forced with the same spatially averaged input. In addition, the spatial fractions of the grassland and wetland HRUs, respectively, were set to 0 and the entire study basin therefore represented by the one HRU which is similar to the forest HRU described in distributed model, similar to many traditional lumped formulations of process-based conceptual models (Bouaziz et al., 2021; Clark et al., 2008; Fenicia et al., 2006; Fovet et al., 2015; Seibert et al., 2010). This implementation has 11 calibration parameters (Table 3).

4.2.2 Spatially distributed model implementation

To balance the need for spatial detail to some extent with the adverse effects of increased parameter uncertainty (e.g. Beven, 2006) and computational capacity (in particular for the calculation of TTDs), we here implemented the integrated model in parallel (IM-SAS-D) in the four precipitation zones P1 – P4 and forced it with the corresponding input (e.g. P, $\delta^{18}O$ and ^{3}H) for each precipitation zone as described in section 3.2. Each precipitation zone was further discretized (1) into 100 m elevation zones for a stratified representation of the snow storage S_{snow} (e.g. Mostbauer et al., 2018) and (2) into three HRUs, i.e., forest, grassland, wetland (Fig.2; e.g. Gharari et al., 2014; Hanus et al., 2021). Rain P_{rain} and melt water M_{snow} from the different elevation zones was aggregated according to their associated spatial weights in each elevation zone. This total liquid water input was then routed through the three parallel HRUs. The classification into the three HRUs was based on the metric Height-above-nearest-drainage (HAND; Gharari et al., 2011) and land cover. While landscape elements with HAND < 5 m were classified as wetland, all other parts of the landscape were classified as forest or grassland according to land-use data. In total, there are therefore 12 individual, parallel model components, i.e., three HRUs in each of the four precipitation zones, not

https://doi.org/10.5194/hess-2022-400
Preprint. Discussion started: 13 December 2022


Hydrology and Earth System Sciences
Discussions

counting the elevation zones for the snow module. All flux and storage variables of the 12 components are weighted according to their areal fractions. While each of the three HRUs was characterized by individual parameters (e.g. Gao et al., 2016; Prenner et al., 2018), the same parameter values were used in all four precipitation zones in distributed moisture accounting approach (e.g. Ajami et al., 2004; Euser et al., 2015; Hulsman et al., 2021b; Roodari et al., 2021). Overall, the spatially distributed implementation has 19 model parameters, including five global parameters (T_t, C_{melt}, C_a, K_s and $S_{s,p}$) that are identical for each HRU and 14 HRU-specific parameters (Table 3; Fig.2).

4.3 Model calibration and post-calibration evaluation

The models were run at a daily time step, whereby the observed volume-weighted monthly tracer concentration in precipitation was used as model input for each day of that month together with the daily data of precipitation. Model performance was evaluated based on the Mean Square Error (MSE) as error metric. The convolution integral models, using uniform prior parameter distributions as shown in Table 3, were individually calibrated to the observed $\delta^{18}O$ (calibration strategy $C_{\delta^{18}O}$; Table 2) and ^3H stream water concentrations ($C_{^3H}$), respectively. In contrast, a multi-objective calibration approach was applied for the integrated model to simultaneously reproduce stream flow volumes and tracer concentrations thereof (e.g. ^3H and/or $\delta^{18}O$). Briefly, the model parameters were calibrated by using Borg_MOEA algorithm (Borg Multi-objective evolutionary algorithm; Hadka and Reed, 2013) and based on uniform prior distributions (Table 3). The model performances were evaluated based on the models' ability to simultaneously reproduce multiple signatures of stream flow as well as signatures of tracer dynamics as shown in Table 2. The sets of pareto optimal solutions obtained from the calibration procedures were then retained as acceptable solutions for the subsequent analysis. To compare the water age distributions (i.e., TTDs and RTDs) and thus to test the research hypothesis, different calibration strategies – $C_{\delta^{18}O,Q}$, $C_{^3H,Q}$ and $C_{\delta^{18}O,^3H,Q}$ – were adopted (Table 2). While in strategy $C_{\delta^{18}O,Q}$ the models were calibrated to simultaneously reproduce signatures of stream flow and $\delta^{18}O$, $C_{^3H,Q}$ combined the stream flow signatures with ^3H. In strategy $C_{\delta^{18}O,^3H,Q}$ the model was finally calibrated to simultaneously reproduce the six stream flow signatures, $\delta^{18}O$, *and* ^3H dynamics. For each strategy, all performance metrics were also combined into an overall performance metric based on the Euclidian distance (D_E), where $D_E = 0$ indicates a perfect fit. To find a somewhat balanced solution in absence of more detailed information all individual performance metrics were here equally weighted (e.g., Hrachowitz et al., 2021; Hulsman et al., 2021b):

$$D_E = \sqrt{\frac{1}{2}\left(\frac{\sum_{n=1}^{N}\left(E_{MSE,Q,n}\right)^2}{N} + \frac{\sum_{m=1}^{M}\left(E_{MSE,tracer,m}\right)^2}{M}\right)}, \quad (14)$$

Where $N = 6$ is the number of performance metrics with respect to stream flow and M is the number of performance metrics for tracers in each combination (e.g. M=1 for $C_{\delta^{18}O,Q}$, and $C_{^3H,Q}$, M=2 for $C_{\delta^{18}O,^3H,Q}$). Note that the different units and thus different magnitudes of residuals introduce some subjectivity in finding the most balanced overall solution according to D_E

https://doi.org/10.5194/hess-2022-400
Preprint. Discussion started: 13 December 2022


Hydrology and Earth System Sciences
Discussions

(Eq. 14). However, a preliminary sensitivity analysis with varying weights for the individual performance metrics in D_E suggested limited influence on the overall results and is thus not further reported here.

After a warm-up period 01/01/1978 – 30/09/2001 the models were calibrated for the 01/10/2001 – 31/12/2009 period. The calibration period was chosen so that observations of all three calibration variables, i.e., Q, ^3H and $\delta^{18}O$, are available for the entire calibration period to allow a consistent comparison. The long model warm-up period was deemed necessary to meaningfully approximate the model initial conditions due to the potential and *a priori* unknown relevance of old water in the study basin, and thus to avoid underestimation of water ages inferred from ^3H data. The pareto optimal solutions (parameter sets) were then used to test the model in the post-calibration evaluation period 01/01/2010 – 31/12/2016. The water age distributions, i.e., TTDs and RTDs, extracted from the individual models and calibration strategies were then estimated based on the corresponding sets of pareto optimal solutions obtained for each calibration strategy.

5 Results

5.1 Model performance

The stream tracer responses of the lumped baseline models were found to be broadly consistent with the available observations (Table 4). For the SW models (Scenarios 1, 2) in particular the sine wave fitted to the stream water $\delta^{18}O$ observations provides a robust characterization of the observed signal with $MSE_{\delta^{18}O}$ = 0.121 and 0.144 ‰ for calibration and model evaluation periods, respectively (Supplementary Material Fig. S5). Similarly, the CO models (Scenarios 3, 5) reproduced the overall pattern of seasonal fluctuations and the degree of dampening of the $\delta^{18}O$ response (Supplementary Material Fig. S6). With $MSE_{\delta^{18}O}$ = 0.213 and 0.245 ‰ for the calibration and model evaluation periods, respectively, the CO-GM model, based on a gamma TTD performed slightly better than the exponential model (CO-EM) with $MSE_{\delta^{18}O}$ = 0.334 and 0.430 ‰. When used with ^3H data in scenarios 4 and 6, the CO models do capture the general decrease in the magnitude of stream water ^3H concentrations although fluctuations at shorter timescales are not well reproduced (Supplementary Material Fig. S7). Both, CO-EM and CO-GM are characterized by $MSE_{^3H} \sim 5$ TU^2 throughout the calibration and evaluation periods. It is also noted that both models already mimic the ^3H response well in the 1978 – 2001 pre-calibration model warm-up period.

In contrast to the above baseline models the implementations of the integrated model IM-SAS (Table 4) aim to not only to reproduce the $\delta^{18}O$ or ^3H stream signals, but to additionally and simultaneously describe the hydrological response (Table 4). Both, the lumped IM-SAS-L (scenario 7; Supplementary Material Fig. S8a, b) and the distributed IM-SAS-D (scenario 10; Fig. 3a, b) reproduce the seasonal fluctuations as well as the degree of dampening of the $\delta^{18}O$ signals with $MSE_{\delta^{18}O}$ = 0.079 – 0.083 ‰ for the calibration and 0.273 – 0.332 ‰ for the evaluation periods similar to or better than the baseline models. The IM-SAS models do also describe the evolution of the ^3H stream signals rather well (scenarios 8 and 11). With $MSE_{^3H} < 3$ TU^2, IM-SAS-L (Supplementary Material Fig. S9) and IM-SAS-D (Fig. 4) do not only outperform the baseline models with respect to the overall magnitude of ^3H, but do, in spite of somewhat underestimating the magnitude of seasonal amplitudes, also provide a better representation of these intra-annual fluctuations. Similar to the above baseline models, the IM-SAS

https://doi.org/10.5194/hess-2022-400
Preprint. Discussion started: 13 December 2022


Hydrology and Earth System Sciences
Discussions

implementations also very well capture the ^{3}H response in the 1978 – 2001 pre-calibration model warm-up period. The simultaneous calibration to the hydrological response, $\delta^{18}O$ *and* ^{3}H stream signals (scenarios 9, 12) led to a comparable model skill to reproduce the tracer signals. In addition to the tracer concentrations, all IM-SAS implementations do also reproduce the main features of the hydrological response (Table 4). More specifically, the modelled hydrographs in particular describe well the timing of peaks as well as the shape of recessions; although in some cases peak flows were underestimated and low flows overestimated as shown for scenario 12 in Figure 5 (for scenarios 7 – 11 see Figs. S10 – S14). The resulting in MSE_Q remains ≤ 0.336 $mm^2\ d^{-2}$ across all IM-SAS implementations (scenarios 7 – 12). Crucially, the models also reproduce well the other observed stream flow signatures such as the flow duration curves ($MSE_{FDCQ} \leq 0.047\ mm^2\ d^{-2}$; Fig. 5d), the seasonal runoff coefficients ($MSE_{RC} \leq 0.008$; Fig. 5e) and the autocorrelation functions ($MSE_{ACQ} \leq 0.007$; Fig. 5f).

5.2 Model parameters

Parameters of the baseline models (scenarios 1 – 6) directly define the shapes of parametric TTDs and thus the associated metrics of water age, such as MTT following Eqs. (3) and (4). The SW and CO models representing $\delta^{18}O$ signals (scenarios 1 – 4) are characterized by parameters that lead to values of β ~ 270 – 1275 d. In comparison, the same models calibrated to ^{3}H (scenarios 5, 6) lead to parameter values β ~ 3795 and 7020 d that are higher by at least a factor of 5 (Table 3).

The individual parameters of the IM-SAS model implementations (scenarios 7 – 12), in contrast, do not directly define parametric TTDs nor can they be readily and directly be linked to water ages. However, it has been previously shown that the sizes of water storage volumes is an important control on water ages (e.g. Harman, 2015) and that in particular hydrologically passive storage volumes, represented in the IM-SAS models by parameter $S_{s,p}$, are key to regulate in particular older water ages in many systems (e.g. Hrachowitz et al., 2016). Calibration of the lumped IM-SAS-L to $\delta^{18}O$ and stream flow ($C_{\delta^{18}O,Q}$) in scenario 7 led to a moderately well identifiable range of this parameter $S_{s,p}$ ~ 4107 – 10029 mm across all pareto optimal solutions (Fig. 6a, Table 3). Reflecting the water storage capacity in the unsaturated root zone, which is an important control on younger water ages (Hrachowitz et al., 2021), the parameter S_{umaxF} was found to range between ~ 314 – 415mm (Fig. 6b, Table 3) for the same scenario. The calibration of the same model to ^{3}H (scenario 8) resulted in a similar ranges for both $S_{s,p}$ ~ 3924 – 9339 mm (Fig. 6a) as well as, albeit slightly lower, S_{umaxF} ~236 – 355 mm (Fig. 6b). The similarities between these two scenarios are also reflected in the parameter ranges obtained from the simultaneous calibration to $\delta^{18}O$ and ^{3}H ($C_{\delta^{18}O,^{3}H,Q}$) in scenario 9. The calibration of the distributed IM-SAS-D model following all the three calibration strategies in scenarios 10 – 12, resulted in values for $S_{s,p}$ ~ 3270 – 9011 mm (Fig. 6c) that are broadly in the similar ranges as for IM-SAS-L ($S_{s,p}$ ~ 3924 – 13676 mm). In contrast, the distinction into the individual HRUs led to clear differences between S_{umaxF}, S_{umaxG} and S_{umaxW} (Figs. 6d-f), reflective of the different hydrological functioning of these HRUs. Nevertheless, the area-weighted average of these parameters comes close to the equivalent parameter from the lumped model implementation (S_{umaxF}). The general consistency of these parameters obtained from the different calibration strategies is exacerbated by the limited differences in the most balanced solutions (smallest D_E) between the different scenarios. For example the most balanced solutions of $S_{s,p}$ fall between ~ 4000 – 5000 mm for all IM-SAS scenarios 7 – 12 (Figs. 6a, c). All other parameters, which are less clearly related

https://doi.org/10.5194/hess-2022-400
Preprint. Discussion started: 13 December 2022


Hydrology and Earth System Sciences
Discussions

505 to water ages, exhibit different levels of variation across the individual scenarios yet not following any clear and systematic pattern (Table 3).

5.3 Water age distributions

Based on a $\delta^{18}O$ amplitude ratio $A_s/A_p = 0.21$ (Table 4), the results of the SW models (scenarios 1, 2) suggest a system that is characterized by rather young stream water with MTT ~ 0.7 – 1.8 yr, depending on the choice of TTD (Table 5; Fig. 7). The
510 TTDs obtained from the CO models calibrated to $\delta^{18}O$ (scenarios 3, 5) are broadly consistent with that, suggesting MTT ~ 1.4 – 1.7 yr. These TTDs suggest mean water ages that are up to ~ 9 yr lower than estimates from CO models calibrated to ^3H (scenarios 4, 6) with MTT ~ 9.6 – 10.4 yr (Table 5; Fig. 7). For higher percentiles the differences in water ages can even reach more than 20 years. Correspondingly, the fractions of younger water F(T < 3 m) exhibit considerable differences of 14 – 17% points between $\delta^{18}O$ and ^3H inferred estimates, which further increase to differences of 39 – 63% for F(T < 3 yr).
515 In contrast, from the implementations of IM-SAS models in scenarios 7 – 12 it can be clearly seen that the stream water ages inferred from $\delta^{18}O$ are across most percentiles by a factor of around 10 higher than those from SW and CO models, resulting in volume-weighted average MTT ~ 16 – 18 yr over the modelling period (Table 5; Fig. 7). Similarly, all water fractions below 20 years are substantially lower for the IM-SAS models than for SW and CO models. The most pronounced difference is observed at F(T < 5 yr) that reaches 38 % for IM-SAS and 91 – 100% for SW and CO, which equals to a difference of more
520 than 50%. These water age estimates from $\delta^{18}O$ in IM-SAS (scenarios 7, 10) models are not only very similar to the estimates from ^3H in these models (scenarios 8, 11) but $\delta^{18}O$ suggests, against the expectations, even slightly *older* water than ^3H does. More specifically, while $\delta^{18}O$ results in stream water MTT > 16 yr, the ^3H-based estimates reach MTT ~ 15 yr and thus one year younger (Table 5; Fig. 7). The differences between $\delta^{18}O$ and ^3H water ages inferred from all IM-SAS model implementations (scenarios 7 – 12) are similar over all percentiles with $\Delta TT_{\delta^{18}O\text{-}^3H}$, on average, not exceeding ~ 2 yr.
525 Accordingly, the fractions of water of any given age up to T < 20 years is ~ 2 – 8 % higher for ^3H than for $\delta^{18}O$, suggesting higher fractions of old water modelled with $\delta^{18}O$ (Table 5). Equivalent pattern and comparable magnitudes are found for the combined use of $\delta^{18}O$ and ^3H in scenarios 9 and 12.

An explicit comparison between the lumped IM-SAS-L (scenarios 7 – 9) and the distributed IM-SAS-D (scenarios 10 – 12) also suggests a good correspondence between the respective inferred water ages for both tracers. While IM-SAS-L generates
530 MTT ~ 13.6 – 18.2 years, the MTT obtained from IM-SAS-D reach ~ 14 – 16 years (Table 5, Fig. 7). Besides the MTT, also the differences in water ages across all percentiles is minor and reaches a maximum of 4.6 years at the 75th percentile. Accordingly, the fractions of water with ages T < 20 yr exhibit only marginal differences between the lumped (IM-SAS-L) and distributed model (IM-SAS-D) implementations.

The consistency between water ages inferred from $\delta^{18}O$ and ^3H, respectively, is further illustrated by the direction and
535 magnitude of change in water age distributions as a consequence of changing wetness conditions. In particular during wet-up and wet periods, a marked variability of daily TTDs can be observed for all scenarios 7 – 12, with young water fractions F(T < 3 m) ranging between ~ 20 – 65% for $\delta^{18}O$-based estimates and ~ 25 – 70% for ^3H (Fig. 8a, b). Less variability in daily TTDs

https://doi.org/10.5194/hess-2022-400
Preprint. Discussion started: 13 December 2022


Hydrology and Earth System Sciences
Discussions

is found under drying and dry conditions with generally F(T < 3 m) in the range of ~ 1 – 20%, with only very few outliers > 30%. Overall, the volume-weighted average TTDs for wet conditions suggest slightly older water inferred from $\delta^{18}O$ with a median water age of ~ 3 year and F(T < 3 m) ~ 30%, for wet conditions than from ^{3}H, for which a median age of ~ 1 year and F(T < 3 m) ~ 40 % were found (Fig. 8d). This is in opposite to dry conditions for which the differences between $\delta^{18}O$ and ^{3}H-derived water age estimates become mostly negligible (Fig. 8d).

With IM-SAS models, not only MTT/TTD in streams can be derived but also in any fluxes/storages (i.e., transpiration flux E_a, ground water storage). An even more pronounced young water variability in daily TTDs was found for the transpiration flux E_a leaving the unsaturated root zone storage S_u in the IM-SAS models (scenarios 7 – 12). As shown in Figure 9a, the transpiration TTDs inferred from $\delta^{18}O$ suggest a median transpiration age during wet conditions of ~ 2 – 40 days and F(T < 3 m) ~ 60 – 100%. This variability shifts to median ages between ~ 30 – 100 days and F(T < 3 m) ~ 30 – 95% for dry conditions. This pattern of variability in daily TTDs in wet and dry periods is very closely matched by the estimates based on ^{3}H (Fig. 9b). Overall, the volume-weighted average TTDs of transpiration suggest median ages of around 14 days for wet conditions and between 35 days (^{3}H) and 70 days ($\delta^{18}O$) for dry conditions (Fig. 9d).

The modelled groundwater, in comparison, was found to be characterized by substantially less temporal variability in TTDs and older water ages (Fig. 10). The TTDs inferred from both, $\delta^{18}O$ and ^{3}H, are similar and characterized by a median age of ~ 10 years under wet and dry conditions. While F(T < 3 m) largely remains < 1%, and ~ 20 – 25 % of the groundwater is older than 20 years.

6 Implications, limitations and unresolved questions

What can we learn from the above? We believe the results obtained in this study have several implications for the utility of different tracer and model types, as described in detail below.

6.1 The individual roles of the choices of tracers and models for underestimation of water ages

The overall magnitude of water ages here estimated from SW and CO models in combination with $\delta^{18}O$ reach MTTs of ~ 2 years (Table 5, Fig.7). These values fall within the age ranges reported for comparable model experiments with seasonally variable tracers in many other catchments world-wide (see McGuire and McDonnell, 2006; Godsey et al., 2009; Hrachowitz et al., 2009; Stewart et al., 2010 and references therein). Similarly, the water ages estimated with the same CO models in combination with ^{3}H are with MTTs ~ 10 yrs by a factor of ~ 5 higher (Table 5, Fig. 7), and also well reflect the findings of previous studies, many of which suggest ^{3}H-inferred catchment MTTs of ~ 10 – 15yr (Stewart et al., 2010 and references therein). This suggests that the Neckar basin does not exhibit unusual or unexpected water age characteristics. By themselves, these results would therefore lend further supporting evidence for the interpretation provided by Stewart et al. (2010) and, crucially, lead us to the same conclusion, that the use of $\delta^{18}O$ and comparable seasonally variable tracers truncate stream water ages.

https://doi.org/10.5194/hess-2022-400
Preprint. Discussion started: 13 December 2022


Hydrology and Earth System Sciences
Discussions

However, and in stark contrast, the estimates of water age obtained from all IM-SAS model implementations in this study, i.e., scenarios 7 – 12, are similar to each other, and most importantly, irrespective of the tracer used. Water ages estimated from $\delta^{18}O$ are, with MTT > 16 yr, not only substantially older than those inferred from the SW and CO models (scenarios 1 – 3, 5), and similar than those inferred from ^{3}H in IM-SAS models, which reach MTT ~ 15 yr (Table 5, Fig. 7). These water ages highlight the importance of old water in the Neckar basin, similar to what is suggested by the use of ^{3}H in CO models (scenarios 4, 6).

It is important to note that the IM-SAS models can simultaneously reproduce several signatures of the hydrological response together with the $\delta^{18}O$ and ^{3}H stream water signals. They therefore provide a more coherent and holistic description of physical transport processes in the system (Table 4, Fig. 3 – 5) than the SW and CO models, which can mimic merely one single tracer signal and thus one isolated variable at a time. In addition, the IM-SAS model parameters that are most linked to tracer circulation, e.g. $S_{s,p}$ and S_{umax} (Fig. 6), exhibit little difference when obtained from calibration to $\delta^{18}O$ or ^{3}H, respectively. This implies that both, $\delta^{18}O$ and ^{3}H, provide similar information about how tracers are routed through the model and how water is stored in and released from the system. As a consequence, also the *simultaneous* representation of all three types of variables under consideration, i.e., the hydrological response as well as the $\delta^{18}O$ and ^{3}H stream signals, in these models is consistent with the observed data (scenarios 9, 12).

The above is further corroborated by how water ages in the Neckar basin respond to changing wetness conditions. Although not identical, $\delta^{18}O$ and ^{3}H-inferred daily TTDs exhibit nevertheless broad agreement in the directions and magnitudes of change in response to changing wetness conditions (Fig. 8). Changes in stream flow TTDs are not primarily caused by changes of water ages within individual storage components. In particular, the modelled water age distributions in the groundwater S_s show limited sensitivity to changing wetness conditions, with MTT varying between ~ 18 years in dry periods and ~ 17 years in wet periods (Fig. 10). The TTDs in the transpiration flux E_a, which are reflective of the water ages in the unsaturated root zone S_u, exhibit with MTTs between ~ 0.20 and 0.12 years in dry and wet periods (Fig. 9), respectively, magnitudes and fluctuations over time that are similar to what has been previously reported in other studies (e.g., Hrachowitz et al., 2015; Soulsby et al., 2016; Visser et al., 2019; Birkel et al., 2020; Kuppel et al., 2020). However, the level of these age fluctuations alone is insufficient to explain the magnitude of change in stream flow TTDs, which can vary by several years. Instead, the temporal variability of stream flow TTDs is largely controlled by switches in the relative contributions of individual storage components to stream flow under different wetness conditions. Under increasingly wet conditions, considerably increasing proportions of comparably young water from S_U contribute over shallow preferential flow pathways (S_F) to stream flow, while the relative proportion of groundwater contributing to stream flow under such conditions is reduced (Hrachowitz et al., 2013). Both tracers, $\delta^{18}O$ and ^{3}H, generate these patterns in a corresponding way.

Altogether, this suggests that the IM-SAS models and the resulting estimates of water ages resulting from both, $\delta^{18}O$ and ^{3}H, provide plausible descriptions of transport processes and thus water ages in the Neckar basin. Clearly, with current observation technology, it is impossible to know the real water age distribution at river basin scale. However, the water ages and their temporal variability inferred from both, $\delta^{18}O$ and ^{3}H using IM-SAS models are widely consistent. In addition, these models

https://doi.org/10.5194/hess-2022-400
Preprint. Discussion started: 13 December 2022


Hydrology and Earth System Sciences
Discussions

can also reproduce the hydrological response. Together, this is suggestive that it is not the use of $\delta^{18}O$ *per se* that leads to truncation of TTDs, but rather that lumped convolution integral models are incapable of extracting meaningful information from $\delta^{18}O$ signals. These results mirror anecdotal evidence from several previous studies (e.g., Hrachowitz et al., 2015, 2021; Ala-aho et al., 2017; Buzacott et al., 2020; Yang et al, 2021). Although no direct comparison with ^{3}H data is provided in these studies, they demonstrated the potential of $\delta^{18}O$ in SAS-based model approaches to estimate water age distributions with considerable fractions of water older than 5 – 10 years and Birkel et al. (2020) explicitly estimated MTTs of up to 18 years. Our results also strongly support the findings and general conclusions of Rodriguez et al. (2021), who undertook a direct comparison of water ages inferred from $\delta^{18}O$ and ^{3}H. In their study for a small catchment and based on shorter tracer time series, i.e., 2 years, and a system that is characterized by rather low MTT of ~ 3 years, they found that although ^{3}H led to higher MTTs than $\delta^{18}O$, the absolute difference between these ages estimates was with 0.2 years limited and even decreasing for higher percentiles of the water age distributions.

We therefore argue that the evidence emerging from our results and the above considerations is strong enough to reject the hypothesis that $\delta^{18}O$ as a tracer generally and systematically "cannot see water older than about 4 years" (Stewart et al., 2010, 2012) and the corresponding tails in water age distributions, leading to underestimations of water ages. We further argue that previous underestimations of water ages are rather a consequence of the use of lumped parameter convolution integral model techniques that cannot resolve the information contained $\delta^{18}O$ signals in a meaningful way for catchments with transient flow conditions. Only the combined information using hydrological and tracer data and the consideration of transient flow conditions gives similar MTT, independent of the used tracer.

However, and notwithstanding the rejection of the above hypothesis it is important to note that overall and in spite of the similarity between $\delta^{18}O$ and ^{3}H inferred water ages in the study basin on the basis of IM-SAS models, there may be no general equivalence between $\delta^{18}O$ and ^{3}H tracers. Instead, it is plausible to assume that differences will gradually increase with higher water ages. In systems characterized by water older than the water in the Neckar study basin, and where the amplitudes of the $\delta^{18}O$ stream signal are attenuated to below the analytical precision, the water age estimates from $\delta^{18}O$ will indeed become subject to increasing uncertainty up to the point where further attenuation and thus older water ages cannot be discerned anymore; independent of modelling approaches. The specific magnitude of such a water age threshold remains difficult to quantify with the available data. However, given the results in the Neckar study basin, the question raised by Stewart et al. (2021), if $\delta^{18}O$ allows to see "the full range of travel times", can to some extent be answered: it can be assumed that, when used with a suitable model, $\delta^{18}O$ contains sufficient information for a meaningful characterization of water ages in systems characterized by MTTs of at least ~15 – 20 years, which encompasses the vast majority of river basins so far analyzed in literature (see Stewart et al., 2010 and references therein). As a step forward, the original hypothesis above can, for future research, be reformulated into: $\delta^{18}O$-inferred water age estimates are subject to increasing uncertainty and bias when compared to ^{3}H-inferred estimates when stream water MTTs of ~ 15 – 20 years are exceeded in systems characterized by increasingly old water.

https://doi.org/10.5194/hess-2022-400
Preprint. Discussion started: 13 December 2022


Hydrology and Earth System Sciences
Discussions

6.2 The role of spatial aggregation on underestimation of water ages

In addition to the above, Kirchner (2016) demonstrated that the use of seasonally variable tracers with lumped parameter model approaches, i.e., SW and CO, has considerable potential to underestimate water ages due to the aggregation of spatially heterogeneous processes. We could here not reproduce that exact experiment, as stream observations were available only at one location for each tracer. However, in the distributed implementation of the IM-SAS-D model (scenarios 10 – 12), we nevertheless explicitly accounted, albeit to a limited degree, for heterogeneity in the system input variables as well as for potential differences in landscape types, as expressed by the three model HRUs. The comparison between the lumped IM-SAS-L (scenarios 7 – 9) and the distributed IM-SAS-D models does not show major differences in their ability to reproduce the various hydrological signatures nor the $\delta^{18}O$ and ^{3}H stream signals (Table 4). Against evidence from various previous studies (e.g., Euser et al., 2015; Gao et al., 2016; Nijzink et al., 2016), this reflects to some degree the conclusion by Loritz et al. (2021), who found in a comparative analysis that distributed model implementations do not improve a model's ability to reproduce the hydrological response as compared to spatially lumped formulations. As a consequence, the results here also do not show significant differences in the associated water age estimates, with MTTs ~ 14 – 18 yrs for IM-SAS-L and 14 – 16 yrs for IM-SAS-D, respectively (Table 5, Fig. 7).

How can this be interpreted? If significantly older ages were inferred from the distributed IM-SAS-D implementation, this would have provided strong supporting evidence for the role and effect of spatial heterogeneity on water ages as demonstrated by Kirchner (2016). However, the similar water ages inferred from the spatially lumped and distributed implementations, respectively, allow two possible but mutually contradicting interpretations. Either, it could indicate that the aggregation of spatial heterogeneity does not have any discernible effect on water ages inferred from the IM-SAS model in the study basin or, on the contrary, the spatial resolution of the model and the available data was not sufficient to detect any significant differences. The evidence found here therefore remains inconclusive and further research is required to describe the role of the aggregation of spatial heterogeneity for estimates of water ages using IM-SAS type of models.

For any estimates of water ages in this study – as in any other study – it is important to bear in mind that they are conditional on the available data and models used. Uncertainties can and do arise from both, data and from decisions taken in the modelling process (e.g., Beven, 2006; Kirchner, 2006). One challenge in this study was that precipitation $\delta^{18}O$ and ^{3}H compositions were only available at rather coarse spatial and temporal resolutions. We have used the best available information to spatially extrapolate the tracer precipitation data from the individual sampling stations to estimate their spatial variation across the Neckar basin including stations outside the study basin. The monthly $\delta^{18}O$ and ^{3}H distribution in precipitation within South-Germany is generally similar (Stumpp et al. 2014; Schmidt et al. 2020); still, regional correction for $\delta^{18}O$ might not be sufficient to explain local differences in $\delta^{18}O$ precipitation data. A similar limitation applies to the temporal resolution of tracer composition in precipitation as only monthly information was available. However, as the available data nevertheless reflect the seasonal variation in $\delta^{18}O$ and ^{3}H precipitation input, the uncertainties arising can be assumed to largely affect the short-term dynamics of tracers in the stream and thus rather young water ages, whereas the objective of our analysis was focused on

https://doi.org/10.5194/hess-2022-400
Preprint. Discussion started: 13 December 2022


Hydrology and Earth System Sciences
Discussions

the right tail of the water age distributions and thus on old ages. Notwithstanding these uncertainties, the overall model performances with respect to the hydrological and tracer responses, suggest that the choice of input data and the model formulations led to model results that are largely consistent with the observed responses in the stream. The observation that there is little ambiguity in the results further suggests that the remaining uncertainties are unlikely to affect the overall interpretation and conclusions of this study.

7 Conclusions

$\delta^{18}O$ and ^{3}H are frequently used as tracers in environmental sciences to estimate age distributions of water. However, it has previously been argued that seasonally variable tracers, such as $\delta^{18}O$, fail to detect the tails of water age distributions and therefore substantially underestimate water ages as compared to radioactive tracers, such as ^{3}H. In this study for the Neckar River basin in central Europe and based on a >20-year record of hydrological, $\delta^{18}O$ and ^{3}H data we systematically scrutinized the above postulate by comparing water age distributions inferred from $\delta^{18}O$ and ^{3}H with a total of 12 different model implementations. The main findings of our analysis are the following:

(1) Water ages inferred from $\delta^{18}O$ with commonly used sine wave (SW) and lumped parameter convolution integral models (CO) are with MTTs ~ 1 – 2 years substantially lower than those obtained from ^{3}H with the same models, reaching MTTs ~ 10 years.

(2) In contrast, integrated hydrological models in combination with the concept of SAS-functions (IM-SAS) did not only allow *simultaneous* representations of stream flow as well as $\delta^{18}O$ and ^{3}H stream signals, but water ages inferred from $\delta^{18}O$ were with MTTs ~ 16 years much higher than those from SW and CO models and even *higher* than inferred from ^{3}H, which suggested MTTs ~ 15 years.

(3) Constraining IM-SAS model implementations individually with $\delta^{18}O$ and ^{3}H observations resulted in similar values for parameters that control water ages, such as the passive groundwater volumes $S_{s,p}$. In addition, $\delta^{18}O$ and ^{3}H-constrained models both exhibited limited differences in the magnitudes of water ages in different parts of the models as well as in the temporal variability of TTDs in response to changing wetness conditions. This suggests that both tracers lead to comparable descriptions of how water is routed through the system.

(4) Based on the points above, we reject the hypothesis that $\delta^{18}O$ as a tracer generally and systematically "cannot see water older than about 4 years" (Stewart et al., 2010, 2012) and that it truncates the corresponding tails in water age distributions, leading to underestimations of water ages.

(5) Instead, our results provide evidence of broad equivalence of $\delta^{18}O$ and ^{3}H as age tracers for systems characterized by MTTs of at least 15 – 20 years.

(6) The question to which degree aggregation of spatial heterogeneity can further adversely affect estimates of water ages remains unresolved as the lumped and distributed implementations of the IM-SAS model provided inconclusive results.

Overall, this study demonstrates that previously reported underestimations of water ages are most likely not a result of the use

of $\delta^{18}O$ or other seasonally variable tracers *per se*. Rather, these underestimations can be largely attributed to the choices of model approaches which rely on assumptions not frequently met in catchment hydrology. Given the vulnerability of lumped parameter convolution integral approaches in combination with $\delta^{18}O$ to substantially underestimate water ages due to transient flow conditions, spatial aggregation and potentially other, still unknown effects, we therefore strongly advocate to avoid the use of this model type in combination with seasonally variable tracers and to instead adopt SAS-based or comparable model formulations.

Code availability. The model code used can be made available by the first author upon request. The equations used in the model are described in supplement.

Data availability. The meteorological and hydrological data used in this study can be obtained from German Weather Service (DWD) and the German Federal Institute of Hydrology (BfG). Both $\delta^{18}O$ and ^{3}H input data used in this study can be obtained from the WISER database portal of the International Atomic Energy Agency (http://www-naweb.iaea.org/napc/ih/IHS_resources_gnip.html). Both $\delta^{18}O$ and ^{3}H output data used in this study can be made available by Christine Stumpp upon request.

Author contributions. SW, MH and GS designed the study, SW executed the experiments, all authors contributed to general idea, the discussion and writing of the manuscript.

Competing interests. Some authors are members of the editorial board of the HESS journal. The peer-review process was guided by an independent editor, and the authors have also no other competing interests to declare.

Disclaimer. Publisher's note: Copernicus Publications remains neutral with regard to jurisdictional claims in published maps and institutional affiliations.

Acknowledgements. We gratefully acknowledge financial support from China Scholarship Council (CSC).

References

Ajami, N. K., Gupta, H., Wagener, T., and Sorooshian, S.: Calibration of a semi-distributed hydrologic model for streamflow estimation along a river system, J. Hydrol., 298, 112–135, https://doi.org/10.1016/j.jhydrol.2004.03.033, 2004.

Ala-Aho, P., Tetzlaff, D., McNamara, J. P., Laudon, H., and Soulsby, C.: Using isotopes to constrain water flux and age estimates in snow-influenced catchments using the STARR (Spatially distributed Tracer-Aided Rainfall–Runoff) model, Hydrol. Earth Syst. Sci., 21, 5089-5110, https://doi.org/10.5194/hess-21-5089-2017, 2017.

Allen, S. T., Kirchner, J. W., and Goldsmith, G. R.: Predicting spatial patterns in precipitation isotope (δ2H and δ18O) seasonality using sinusoidal isoscapes, Geophysical Research Letters, 45, 4859-4868, https://doi.org/10.1029/2018GL077458, 2018.

Allen, S. T., Jasechko, S., Berghuijs, W. R., Welker, J. M., Goldsmith, G. R., and Kirchner, J. W.: Global sinusoidal seasonality in precipitation isotopes, Hydrol. Earth Syst. Sci., 23, 3423-3436, https://doi.org/10.5194/hess-23-3423-2019, 2019.

Asadollahi, M., Stumpp, C., Rinaldo, A., and Benettin, P.: Transport and water age dynamics in soils: A comparative study of spatially integrated and spatially explicit models, Water Resour. Res., 56, e2019WR025539, https://doi.org/10.1029/2019WR0255, 2020.

Begemann, F. and Libby, W. F.: Continental water balance, ground water inventory and storage times, surface ocean mixing rates and world-wide water circulation patterns from cosmic-ray and bomb tritium, Geochimica et Cosmochimica Acta, 12, 277-296, https://doi.org/10.1016/0016-7037(57)90040-6 ,1957.

Benettin, P., Kirchner, J. W., Rinaldo, A., and Botter, G.: Modeling chloride transport using travel time distributions at Plynlimon, Wales, Water Resour. Res., 51, 3259-3276, https://doi.org/10.1002/2014WR016600, 2015a.

Benettin, P., Soulsby, C., Birkel, C., Tetzlaff, D., Botter, G., and Rinaldo, A.: Using SAS functions and high-resolution isotope data to unravel travel time distributions in headwater catchments, Water Resour. Res., 53, 1864-1878, https://doi.org/10.1002/2016WR020117, 2017.

Benettin, P., Nehemy, M. F., Asadollahi, M., Pratt, D., Bensimon, M., McDonnell, J. J., and Rinaldo, A.: Tracing and closing the water balance in a vegetated lysimeter, Water Resour. Res., 57, e2020WR029049, https://doi.org/10.1029/2020WR029049, 2021.

Benettin, P., Bailey, S. W., Campbell, J. L., Green, M. B., Rinaldo, A., Likens, G. E., McGuire, K. J., and Botter, G.: Linking water age and solute dynamics in streamflow at the Hubbard Brook Experimental Forest, NH, USA, Water Resour. Res., 51, 9256-9272, https://doi.org/10.1002/2015WR017552, 2015b

Benettin, P., Rodriguez, N. B., Sprenger, M., Kim, M., Klaus, J., Harman, C. J., Van Der Velde, Y., Hrachowitz, M., Botter, G., McGuire, K. J., Kirchner, J. W., Rinaldo A., McDonnell, J. J.: Transit time estimation in catchments: Recent developments and future directions, Water Resour. Res., https://doi.org/10.1029/2022WR033096, 2022

Beven, K.: Searching for the Holy Grail of scientific hydrology: Q t=(S, R, Δt) A as closure, Hydrol. Earth Syst. Sci., 10, 609-618, https://doi.org/10.5194/hess-10-609-2006, 2006.

Birkel, C., Soulsby, C., and Tetzlaff, D.: Modelling catchment-scale water storage dynamics: Reconciling dynamic storage with tracer-inferred passive storage, Hydrol. Process., 25, 3924-3936, https://doi.org/10.1002/hyp.8201, 2011.

Birkel, C., Soulsby, C., and Tetzlaff, D.: Conceptual modelling to assess how the interplay of hydrological connectivity, catchment storage and tracer dynamics controls nonstationary water age estimates, Hydrol. Process., 29, 2956-2969, https://doi.org/10.1002/hyp.10414, 2015.

Birkel, C., Dunn, S., Tetzlaff, D., and Soulsby, C.: Assessing the value of high-resolution isotope tracer data in the stepwise development of a lumped conceptual rainfall–runoff model, Hydrol. Process., 24, 2335-2348, https://doi.org/10.1002/hyp.7763,

2010.

Birkel, C., Duvert, C., Correa, A., Munksgaard, N. C., Maher, D. T., and Hutley, L. B.: Tracer-aided modeling in the low-relief, wet-dry tropics suggests water ages and DOC export are driven by seasonal wetlands and deep groundwater, Water Resour. Res., 56, e2019WR026175, https://doi.org/10.1029/2019WR026175, 2020.

Botter, G., Bertuzzo, E., and Rinaldo, A.: Catchment residence and travel time distributions: The master equation, Geophys. Res. Lett., 38, https://doi.org/10.1029/2011GL047666, 2011.

Bouaziz, L. J., Fenicia, F., Thirel, G., de Boer-Euser, T., Buitink, J., Brauer, C. C., De Niel, J., Dewals, B. J., Drogue, G., and Grelier, B.: Behind the scenes of streamflow model performance, Hydrol. Earth Syst. Sci., 25, 1069-1095, https://doi.org/10.5194/hess-25-1069-2021, 2021.

Buzacott, A. J., van Der Velde, Y., Keitel, C., and Vervoort, R. W.: Constraining water age dynamics in a south-eastern Australian catchment using an age-ranked storage and stable isotope approach, Hydrol. Process., 34, 4384-4403, https://doi.org/10.1002/hyp.13880, 2020.

Clark, M. P., Rupp, D. E., Woods, R. A., Zheng, X., Ibbitt, R. P., Slater, A. G., Schmidt, J., and Uddstrom, M. J.: Hydrological data assimilation with the ensemble Kalman filter: Use of streamflow observations to update states in a distributed hydrological model, Adv. Water Resour., 31, 1309-1324, https://doi.org/10.1016/j.advwatres.2008.06.005, 2008.

DeWalle, D., Edwards, P., Swistock, B., Aravena, R., and Drimmie, R.: Seasonal isotope hydrology of three Appalachian forest catchments, Hydrol. Process., 11, 1895-1906, https://doi.org/10.1002/(SICI)1099-1085(199712)11:15<1895::AID-HYP538>3.0.CO;2-%23, 1997.

Dincer, T., Payne, B., Florkowski, T., Martinec, J., and Tongiorgi, E.: Snowmelt runoff from measurements of tritium and oxygen-18, Water Resour. Res., 6, 110-124, https://doi.org/10.1029/WR006i001p00110, 1970.

Duvert, C., Stewart, M., Cendón, D., and Raiber, M.: Time series of tritium, stable isotopes and chloride reveal short-term variations in groundwater contribution to a stream, Hydrol. Earth Syst. Sci., 20, 257-277, https://doi.org/10.5194/hess-20-257-2016, 2016.

Eriksson, E.: The possible use of tritium'for estimating groundwater storage, Tellus, 10, 472-478, https://doi.org/10.3402/tellusa.v10i4.9265, 1958.

Euser, T., Hrachowitz, M., Winsemius, H. C., and Savenije, H. H.: The effect of forcing and landscape distribution on performance and consistency of model structures, Hydrol. Process., 29, 3727-3743, https://doi.org/10.1002/hyp.10445, 2015.

Fenicia, F., Savenije, H., Matgen, P., and Pfister, L.: Is the groundwater reservoir linear? Learning from data in hydrological modelling, Hydrol. Earth Syst. Sci., 10, 139-150, https://doi.org/10.5194/hess-10-139-2006, 2006.

Fenicia, F., Wrede, S., Kavetski, D., Pfister, L., Hoffmann, L., Savenije, H. H., and McDonnell, J. J.: Assessing the impact of mixing assumptions on the estimation of streamwater mean residence time, Hydrol. Process., 24, 1730-1741, https://doi.org/10.1002/hyp.7595, 2010.

Fovet, O., Ruiz, L., Hrachowitz, M., Faucheux, M., and Gascuel-Odoux, C.: Hydrological hysteresis and its value for assessing process consistency in catchment conceptual models, Hydrol. Earth Syst. Sci., 19, 105-123, https://doi.org/10.5194/hess-19-

105-2015, 2015.

Gallart, F., Roig-Planasdemunt, M., Stewart, M. K., Llorens, P., Morgenstern, U., Stichler, W., Pfister, L., and Latron, J.: A GLUE-based uncertainty assessment framework for tritium-inferred transit time estimations under baseflow conditions, Hydrol. Process., 30, 4741-4760, https://doi.org/10.1002/hyp.10991, 2016.

Gao, H., Ding, Y., Zhao, Q., Hrachowitz, M., and Savenije, H. H.: The importance of aspect for modelling the hydrological response in a glacier catchment in Central Asia, Hydrol. Process., 31, 2842-2859, https://doi.org/10.1002/hyp.11224, 2017.

Gao, H., Hrachowitz, M., Fenicia, F., Gharari, S., and Savenije, H.: Testing the realism of a topography-driven model (FLEX-Topo) in the nested catchments of the Upper Heihe, China, Hydrol. Earth Syst. Sci., 18, 1895-1915, https://doi.org/10.5194/hess-18-1895-2014, 2014.

Gao, H., Hrachowitz, M., Sriwongsitanon, N., Fenicia, F., Gharari, S., and Savenije, H. H.: Accounting for the influence of vegetation and landscape improves model transferability in a tropical savannah region, Water Resour. Res., 52, 7999-8022, https://doi.org/10.1002/2016WR019574, 2016.

Gharari, S., Hrachowitz, M., Fenicia, F., and Savenije, H.: Hydrological landscape classification: investigating the performance of HAND based landscape classifications in a central European meso-scale catchment, Hydrol. Earth Syst. Sci., 15, 3275-3291, https://doi.org/10.5194/hess-15-3275-2011, 2011.

Gharari, S., Hrachowitz, M., Fenicia, F., Gao, H., and Savenije, H.: Using expert knowledge to increase realism in environmental system models can dramatically reduce the need for calibration, Hydrol. Earth Syst. Sci., 18, 4839-4859, https://doi.org/10.5194/hess-18-4839-2014, 2014.

Girons Lopez, M., Vis, M. J., Jenicek, M., Griessinger, N., and Seibert, J.: Assessing the degree of detail of temperature-based snow routines for runoff modelling in mountainous areas in central Europe, Hydrol. Earth Syst. Sci., 24, 4441-4461, https://doi.org/10.5194/hess-24-4441-2020, 2020.

Godsey, S. E., Kirchner, J. W., and Clow, D. W.: Concentration–discharge relationships reflect chemostatic characteristics of US catchments, Hydrol. Process., 23, 1844-1864, https://doi.org/10.1002/hyp.7315, 2009.

Godsey, S. E., Aas, W., Clair, T. A., De Wit, H. A., Fernandez, I. J., Kahl, J. S., Malcolm, I. A., Neal, C., Neal, M., and Nelson, S. J.: Generality of fractal 1/f scaling in catchment tracer time series, and its implications for catchment travel time distributions, Hydrol. Process., 24, 1660-1671, https://doi.org/10.1002/hyp.7677, 2010.

Goovaerts, P.: Geostatistical approaches for incorporating elevation into the spatial interpolation of rainfall, J. Hydrol., 228, 113-129, https://doi.org/10.1016/S0022-1694(00)00144-X, 2000.

Hadka, D. and Reed, P.: Borg: An auto-adaptive many-objective evolutionary computing framework, Evolutionary computation, 21, 231-259, https://doi.org/10.1162/EVCO_a_00075, 2013.

Hanus, S., Hrachowitz, M., Zekollari, H., Schoups, G., Vizcaino, M., and Kaitna, R.: Future changes in annual, seasonal and monthly runoff signatures in contrasting Alpine catchments in Austria, Hydrol. Earth Syst. Sci., 25, 3429-3453, https://doi.org/10.5194/hess-25-3429-2021, 2021.

Harman, C. J.: Time-variable transit time distributions and transport: Theory and application to storage-dependent transport of

chloride in a watershed, Water Resour. Res., 51, 1-30, https://doi.org/10.1002/2014WR015707, 2015.

Harms, P. A., Visser, A., Moran, J. E., and Esser, B. K.: Distribution of tritium in precipitation and surface water in California, J. Hydrol., 534, 63-72, https://doi.org/10.1016/j.jhydrol.2015.12.046, 2016.

Hrachowitz, M., Fovet, O., Ruiz, L., and Savenije, H. H.: Transit time distributions, legacy contamination and variability in biogeochemical 1/fα scaling: how are hydrological response dynamics linked to water quality at the catchment scale?, Hydrol. Process., 29, 5241-5256, https://doi.org/10.1002/hyp.10546, 2015.

Hrachowitz, M., Savenije, H., Bogaard, T., Tetzlaff, D., and Soulsby, C.: What can flux tracking teach us about water age distribution patterns and their temporal dynamics?, Hydrol. Earth Syst. Sci., 17, 533-564, https://doi.org/10.5194/hess-17-533-2013, 2013.

Hrachowitz, M., Soulsby, C., Tetzlaff, D., Dawson, J. J. C., and Malcolm, I.: Regionalization of transit time estimates in montane catchments by integrating landscape controls, Water Resour. Res., 45, https://doi.org/10.1029/2008WR007496, 2009a.

Hrachowitz, M., Soulsby, C., Tetzlaff, D., Malcolm, I., and Schoups, G.: Gamma distribution models for transit time estimation in catchments: Physical interpretation of parameters and implications for time-variant transit time assessment, Water Resour. Res., 46, https://doi.org/10.1029/2010WR009148, 2010.

Hrachowitz, M., Soulsby, C., Tetzlaff, D., Dawson, J. J. C., Dunn, S., and Malcolm, I.: Using long-term data sets to understand transit times in contrasting headwater catchments, J. Hydrol., 367, 237-248, https://doi.org/10.1016/j.jhydrol.2009.01.001, 2009b.

Hrachowitz, M., Stockinger, M., Coenders-Gerrits, M., van der Ent, R., Bogena, H., Lücke, A., and Stumpp, C.: Reduction of vegetation-accessible water storage capacity after deforestation affects catchment travel time distributions and increases young water fractions in a headwater catchment, Hydrol. Earth Syst. Sci., 25, 4887-4915, https://doi.org/10.5194/hess-25-4887-2021, 2021.

Hrachowitz, M., Benettin, P., Van Breukelen, B. M., Fovet, O., Howden, N. J., Ruiz, L., Van Der Velde, Y., and Wade, A. J.: Transit times—The link between hydrology and water quality at the catchment scale, WIRES Water, 3, 629-657, https://doi.org/10.1002/wat2.1155, 2016.

Hulsman, P., Hrachowitz, M., and Savenije, H. H.: Improving the representation of long-term storage variations with conceptual hydrological models in data-scarce regions, Water Resour. Res., 57, e2020WR028837, https://doi.org/10.1029/2020WR028837, 2021a.

Hulsman, P., Savenije, H. H., and Hrachowitz, M.: Learning from satellite observations: increased understanding of catchment processes through stepwise model improvement, Hydrol. Earth Syst. Sci., 25, 957-982, https://doi.org/10.5194/hess-25-957-2021, 2021b.

IAEA/WMO. Global Network of Isotopes in Precipitation. The GNIP Database. Accessible at: https://nucleus.iaea.org/wiser, 2022.

Kendall, C. and McDonnell, J. J.: Isotope tracers in catchment hydrology, Elsevier, 2012.

Kim, M., Volkmann, T. H., Wang, Y., Meira Neto, A. A., Matos, K., Harman, C. J., and Troch, P. A.: Direct Observation of

Hillslope Scale StorAge Selection Functions in Experimental Hydrologic Systems: Geomorphologic Structure and Preferential Discharge of Old Water, Water Resour. Res., 58, e2020WR028959, https://doi.org/10.1029/2020WR028959, 2022.

Kirchner, J. W.: Getting the right answers for the right reasons: Linking measurements, analyses, and models to advance the science of hydrology, Water Resour. Res., 42, https://doi.org/10.1029/2005WR004362, 2006.

Kirchner, J. W.: Aggregation in environmental systems–Part 1: Seasonal tracer cycles quantify young water fractions, but not mean transit times, in spatially heterogeneous catchments, Hydrol. Earth Syst. Sci., 20, 279-297, https://doi.org/10.5194/hess-20-279-2016, 2016.

Kirchner, J. W., Feng, X., and Neal, C.: Catchment-scale advection and dispersion as a mechanism for fractal scaling in stream tracer concentrations, J. Hydrol., 254, 82-101, https://doi.org/10.1016/S0022-1694(01)00487-5, 2001.

Kirchner, J. W., Tetzlaff, D., and Soulsby, C.: Comparing chloride and water isotopes as hydrological tracers in two Scottish catchments, Hydrol. Process., 24, 1631-1645, https://doi.org/10.1002/hyp.7676, 2010.

Koeniger P, Stumpp C, Schmidt A.: Stable isotope patterns of German rivers with aspects on scales, continuity and network status, Isotopes in Environmental and Health Studies, 1-17, https://doi.org/10.1080/10256016.2022.2127702, 2022.

Kreft, A. and Zuber, A.: On the physical meaning of the dispersion equation and its solutions for different initial and boundary conditions, Chemical Engineering Science, 33, 1471-1480, https://doi.org/10.1016/0009-2509(78)85196-3, 1978.

Kuppel, S., Tetzlaff, D., Maneta, M. P., and Soulsby, C.: EcH 2 O-iso 1.0: Water isotopes and age tracking in a process-based, distributed ecohydrological model, Geoscientific Model Development, 11, 3045-3069, https://doi.org/10.5194/gmd-11-3045-2018, 2018.

Kuppel, S., Tetzlaff, D., Maneta, M. P., and Soulsby, C.: Critical zone storage controls on the water ages of ecohydrological outputs, Geophys. Res. Lett., 47, e2020GL088897, https://doi.org/10.1029/2020GL088897, 2020.

Lloyd, C.: Assessing the effect of integrating elevation data into the estimation of monthly precipitation in Great Britain, J. Hydrol., 308, 128-150, https://doi.org/10.1016/j.jhydrol.2004.10.026, 2005.

Loritz, R., Hrachowitz, M., Neuper, M., and Zehe, E.: The role and value of distributed precipitation data in hydrological models. Hydrol. Earth Syst. Sci., *25*, 147-167, https://doi.org/10.5194/hess-25-147-2021, 2021.

Małoszewski, P. and Zuber, A.: Determining the turnover time of groundwater systems with the aid of environmental tracers: 1. Models and their applicability, J. Hydrol., 57, 207-231, https://doi.org/10.1016/0022-1694(82)90147-0, 1982.

Małoszewski, P., Rauert, W., Stichler, W., and Herrmann, A.: Application of flow models in an alpine catchment area using tritium and deuterium data, J. Hydrol., 66, 319-330, https://doi.org/10.1016/0022-1694(83)90193-2, 1983.

McDonnell, J. J. and Beven, K.: Debates—The future of hydrological sciences: A (common) path forward? A call to action aimed at understanding velocities, celerities and residence time distributions of the headwater hydrograph, Water Resour. Res., 50, 5342-5350, https://doi.org/10.1002/2013WR015141, 2014.

McGuire, K. J. and McDonnell, J. J.: A review and evaluation of catchment transit time modeling, J. Hydrol., 330, 543-563, https://doi.org/10.1016/j.jhydrol.2006.04.020, 2006.

Michel, R. L., Aggarwal, P., Araguas-Araguas, L., Kurttas, T., Newman, B. D., and Vitvar, T.: A simplified approach to

analysing historical and recent tritium data in surface waters, Hydrol. Process., 29, 572-578, https://doi.org/10.1002/hyp.10174, 2015.

Morgenstern, U., Stewart, M. K., and Stenger, R.: Dating of streamwater using tritium in a post nuclear bomb pulse world: continuous variation of mean transit time with streamflow, Hydrol. Earth Syst. Sci., 14, 2289-2301, https://doi.org/10.5194/hess-14-2289-2010, 2010.

Mostbauer, K., Kaitna, R., Prenner, D., and Hrachowitz, M.: The temporally varying roles of rainfall, snowmelt and soil moisture for debris flow initiation in a snow-dominated system, Hydrol. Earth Syst. Sci., 22, 3493-3513, https://doi.org/10.5194/hess-22-3493-2018, 2018.

Nijzink, R., Hutton, C., Pechlivanidis, I., Capell, R., Arheimer, B., Freer, J., Han, D., Wagener, T., McGuire, K., and Savenije, H.: The evolution of root-zone moisture capacities after deforestation: a step towards hydrological predictions under change?, Hydrol. Earth Syst. Sci., 20, 4775-4799, https://doi.org/10.5194/hess-20-4775-2016, 2016.

Pfister, L., Martínez-Carreras, N., Hissler, C., Klaus, J., Carrer, G. E., Stewart, M. K., and McDonnell, J. J.: Bedrock geology controls on catchment storage, mixing, and release: A comparative analysis of 16 nested catchments, Hydrol. Process., 31, 1828-1845, https://doi.org/10.1002/hyp.11134, 2017.

Prenner, D., Kaitna, R., Mostbauer, K., and Hrachowitz, M.: The value of using multiple hydrometeorological variables to predict temporal debris flow susceptibility in an alpine environment, Water Resour. Res., 54, 6822-6843, https://doi.org/10.1029/2018WR022985, 2018.

Rank, D., Wyhlidal, S., Schott, K., Weigand, S., and Oblin, A.: Temporal and spatial distribution of isotopes in river water in Central Europe: 50 years experience with the Austrian network of isotopes in rivers, Isotopes in Environmental and Health Studies, 54, 115-136, https://doi.org/10.1080/10256016.2017.1383906, 2018.

Reckerth, A., Stichler, W., Schmidt, A., and Stumpp, C.: Long-term data set analysis of stable isotopic composition in German rivers, J. Hydrol., 552, 718-731, https://doi.org/10.1016/j.jhydrol.2017.07.022, 2017.

Rinaldo, A., Benettin, P., Harman, C. J., Hrachowitz, M., McGuire, K. J., Van Der Velde, Y., Bertuzzo, E., and Botter, G.: Storage selection functions: A coherent framework for quantifying how catchments store and release water and solutes, Water Resour. Res., 51, 4840-4847, https://doi.org/10.1002/2015WR017273, 2015.

Rodriguez, N. B. and Klaus, J.: Catchment travel times from composite StorAge Selection functions representing the superposition of streamflow generation processes, Water Resour. Res. 55, 9292-9314, https://doi.org/10.1029/2019WR024973, 2019.

Rodriguez, N. B., McGuire, K. J., and Klaus, J.: Time-varying storage–water age relationships in a catchment with a Mediterranean climate, Water Resour. Res., 54, 3988-4008, https://doi.org/10.1029/2017WR021964, 2018.

Rodriguez, N. B., Pfister, L., Zehe, E., and Klaus, J.: A comparison of catchment travel times and storage deduced from deuterium and tritium tracers using StorAge Selection functions, Hydrol. Earth Syst. Sci., 25, 401-428, https://doi.org/10.5194/hess-25-401-2021, 2021.

Roodari, A., Hrachowitz, M., Hassanpour, F., and Yaghoobzadeh, M.: Signatures of human intervention–or not? Downstream

intensification of hydrological drought along a large Central Asian river: the individual roles of climate variability and land use change, Hydrol. Earth Syst. Sci., 25, 1943-1967, https://doi.org/10.5194/hess-25-1943-2021, 2021.

Rozanski, K., Gonfiantini, R., and Araguas-Araguas, L.: Tritium in the global atmosphere: Distribution patterns and recent trends, Journal of Physics G: Nuclear and Particle Physics, 17, S523, 1991.

Schmidt, A., Frank, G., Stichler, W., Duester, L., Steinkopff, T., and Stumpp, C.: Overview of tritium records from precipitation and surface waters in Germany, Hydrol. Process., 34, 1489-1493, https://doi.org/10.1002/hyp.13691, 2020.

Seeger, S. and Weiler, M.: Reevaluation of transit time distributions, mean transit times and their relation to catchment topography, Hydrol. Earth Syst. Sci., 18, 4751-4771, https://doi.org/10.5194/hess-18-4751-2014, 2014.

Seibert, J., McDonnell, J. J., and Woodsmith, R. D.: Effects of wildfire on catchment runoff response: a modelling approach to detect changes in snow-dominated forested catchments, Hydrology research, 41, 378-390, https://doi.org/10.2166/nh.2010.036, 2010.

Shaw, S. B., Harpold, A. A., Taylor, J. C., and Walter, M. T.: Investigating a high resolution, stream chloride time series from the Biscuit Brook catchment, Catskills, NY, J. Hydrol., 348, 245-256, https://doi.org/10.1016/j.jhydrol.2007.10.009, 2008.

Soulsby, C., Birkel, C., and Tetzlaff, D.: Characterizing the age distribution of catchment evaporative losses, Hydrol. Process., 30, 1308-1312, https://doi.org/10.1002/hyp.10751, 2016.

Sprenger, M., Stumpp, C., Weiler, M., Aeschbach, W., Allen, S. T., Benettin, P., Dubbert, M., Hartmann, A., Hrachowitz, M., and Kirchner, J. W.: The demographics of water: A review of water ages in the critical zone, Reviews of Geophysics, 57, 800-834, https://doi.org/10.1029/2018RG000633, 2019.

Stewart, M. and Thomas, J.: A conceptual model of flow to the Waikoropupu Springs, NW Nelson, New Zealand, based on hydrometric and tracer (^{18}O, Cl^-, ^3H and CFC) evidence, Hydrol. Earth Syst. Sci., 12, 1-19, https://doi.org/10.5194/hess-12-1-2008, 2008.

Stewart, M., Morgenstern, U., McDonnell, J., and Pfister, L.: The'hidden streamflow'challenge in catchment hydrology: a call to action for stream water transit time analysis, Hydrol. Process., 26, 2061-2066, https://doi.org/10.1002/hyp.9262, 2012.

Stewart, M. K. and Morgenstern, U.: Importance of tritium-based transit times in hydrological systems, WIRES Water, 3, 145-154, https://doi.org/10.1002/wat2.1134, 2016.

Stewart, M. K., Mehlhorn, J., and Elliott, S.: Hydrometric and natural tracer (oxygen-18, silica, tritium and sulphur hexafluoride) evidence for a dominant groundwater contribution to Pukemanga Stream, New Zealand, Hydrol. Process., 21, 3340-3356, https://doi.org/10.1002/hyp.6557, 2007.

Stewart, M. K., Morgenstern, U., and McDonnell, J. J.: Truncation of stream residence time: how the use of stable isotopes has skewed our concept of streamwater age and origin, Hydrol. Process., 24, 1646-1659, https://doi.org/10.1002/hyp.7576, 2010.

Stewart, M. K., Morgenstern, U., and Cartwright, I.: Comment on "A comparison of catchment travel times and storage deduced from deuterium and tritium tracers using StorAge Selection functions" by Rodriguez et al.(2021), Hydrology and Earth System Sciences, 25, 6333-6338, https://doi.org/10.5194/hess-25-6333-2021, 2021.

Stumpp, C., Klaus, J., and Stichler, W.: Analysis of long-term stable isotopic composition in German precipitation, J. Hydrol., 517, 351-361, https://doi.org/10.1016/j.jhydrol.2014.05.034, 2014.

Tadros, C. V., Hughes, C. E., Crawford, J., Hollins, S. E., and Chisari, R.: Tritium in Australian precipitation: A 50 year record, J. Hydrol., 513, 262-273, https://doi.org/10.1016/j.jhydrol.2014.03.031, 2014.

Uhlenbrook, S., Frey, M., Leibundgut, C., and Maloszewski, P.: Hydrograph separations in a mesoscale mountainous basin at event and seasonal timescales, Water Resour. Res., 38, 31-31-31-14, https://doi.org/10.1029/2001WR000938, 2002.

Van Der Velde, Y., Torfs, P., Van Der Zee, S., and Uijlenhoet, R.: Quantifying catchment-scale mixing and its effect on time-varying travel time distributions, Water Resour. Res., 48, https://doi.org/10.1029/2011WR011310, 2012.

Van Der Velde, Y., Heidbüchel, I., Lyon, S. W., Nyberg, L., Rodhe, A., Bishop, K., and Troch, P. A.: Consequences of mixing assumptions for time-variable travel time distributions, Hydrol. Process., 29, 3460-3474, https://doi.org/10.1002/hyp.10372, 2015.

Visser, A., Thaw, M., Deinhart, A., Bibby, R., Safeeq, M., Conklin, M., Esser, B., and Van der Velde, Y.: Cosmogenic isotopes unravel the hydrochronology and water storage dynamics of the Southern Sierra Critical Zone, Water Resour. Res., 55, 1429-1450, https://doi.org/10.1029/2018WR023665, 2019.

Vitvar, T. and Balderer, W.: Estimation of mean water residence times and runoff generation by180 measurements in a Pre-Alpine catchment (Rietholzbach, Eastern Switzerland), Applied Geochemistry, 12, 787-796, https://doi.org/10.1016/S0883-2927(97)00045-0, 1997.

Yang, D., Yang, Y., and Xia, J.: Hydrological cycle and water resources in a changing world: A review, Geography and Sustainability, 2, 115-122, https://doi.org/10.1016/j.geosus.2021.05.003, 2021.

https://doi.org/10.5194/hess-2022-400
Preprint. Discussion started: 13 December 2022

Hydrology and Earth System Sciences
Discussions
Open Access
EGU

Table1. Characteristics of the Neckar catchment in Germany

Characteristics	
latitude (N)	48°02′00″-49°33′45″
longitude (E)	8°18′45″-10°18′45″
Area (km^2)	13,041
Average annual precipitation (mm yr^{-1})	909
Average annual temperature (°C)	8.9
Elevation range (m)	122-1019
Mean elevation (m)	569
Slope range (°)	0-53
Mean slope (°)	5.1
Forest dominated land (%)	38.1
Grass dominated land (%)	51.2
Wetland (%)	10.7

Table 2. The 12 model scenarios here implemented for the Neckar study basin together with the associated calibration strategies, the individual calibration performance metrics and the type of spatial implementation (lumped or distributed). SW indicates sine-wave models, CO indicates lumped parameter convolution integral models and IM-SAS indicates the integrated hydrological model based on SAS-functions. EM represents an exponential TTD (i.e. α = 1) and GM indicates a gamma TTD with α = 0.5. The symbols L and D indicate lumped and distributed model implementations, respectively. The calibration strategies show which variables/signatures a model was simultaneously calibrated to using the Mean Square Error (MSE) with $C_{\delta^{18}O}$ calibration to only the observed stream water $\delta^{18}O$ signal; C^3_H calibration to only stream water ^3H; $C_{\delta^{18}O,Q}$ simultaneous calibration to $\delta^{18}O$ and six signatures of stream flow Q; $C^3_{H,Q}$ simultaneous calibration to ^3H and the signatures of Q; $C_{\delta^{18}O,^3H,Q}$ the simultaneous calibration to $\delta^{18}O$, ^3H and the signatures of Q. *) Note, that for SW models calibration involves least-square fits of sine waves to both, the precipitation and stream flow signals available.

	Scenario		1	2	3	4	5	6	7	8	9	10	11	12
	Model		SW-EM	SW-GM	CO-EM		CO-GM		IM-SAS-L			IM-SAS-D		
	Implementation		Lumped									Distributed		
	Signature	Calibration strategy → Performance metric ↓	C_x *)	C_x *)	$C_{\delta^{18}O}$	C^3_H	$C_{\delta^{18}O}$	C^3_H	$C_{\delta^{18}O,Q}$	$C^3_{H,Q}$	$C_{\delta^{18}O,^3H,Q}$	$C_{\delta^{18}O,Q}$	$C^3_{H,Q}$	$C_{\delta^{18}O,^3H,Q}$
Performance metrics	Times series $\delta^{18}O$ in stream flow	$MSE_{\delta^{18}O}$	•	•	•	-	•	-	•	-	•	•	-	•
	Time series ^3H in stream flow	$MSE_{^3H}$	-	-	-	•	-	•	-	•	•	-	•	•
	Time series of stream flow (Q)	MSE_Q	-	-	-	-	-	-	•	•	•	•	•	•
	Time series of log(Q)	$MSE_{log(Q)}$	-	-	-	-	-	-	•	•	•	•	•	•
	Flow duration curve of Q (FDC_Q)	MSE_{FDC_Q}	-	-	-	-	-	-	•	•	•	•	•	•
	Flow duration curve log(Q) ($FDC_{log(Q)}$)	$MSE_{FDC_{log(Q)}}$	-	-	-	-	-	-	•	•	•	•	•	•
	Seasonal runoff coefficient (RC)	MSE_{RC}	-	-	-	-	-	-	•	•	•	•	•	•
	Autocorrelation function of Q (AC_Q)	MSE_{AC_Q}	-	-	-	-	-	-	•	•	•	•	•	•

https://doi.org/10.5194/hess-2022-400
Preprint. Discussion started: 13 December 2022

Hydrology and Earth System Sciences
Discussions

Table 3. Parameter prior ranges and pareto optimal ranges (5th/95th percentiles) for each model scenario. Note that *) for the parameters of the SW models, A_p and A_s, no prior distribution was explicitly defined as they are determined by least-squares fits. **) the CO models were calibrated using a single objective function, therefore the set of pareto optimal solution collapses to one optimal solution.

Scenario		1	2	3	4	5	6	7	8	9	10	11	12
Model		SW-EM	SW-GM	CO-EM		CO-GM		IM-SAS-L			IM-SAS-D		
Calibration strategy		C_x	C_x	$C_{\delta^{18}O}$	C^3_H	$C_{\delta^{18}O}$	C^3_H	$C_{\delta^{18}O,Q}$	$C^3_{H,Q}$	$C_{\delta^{18}O,^3H,Q}$	$C_{\delta^{18}O,Q}$	$C^3_{H,Q}$	$C_{\delta^{18}O,^3H,Q}$
Parameter	Prior range	Pareto optimal range											
A_p (‰)	-*	2.69		-	-	-	-	-	-	-	-	-	-
A_s (‰)	-*	0.57		-	-	-	-	-	-	-	-	-	-
β (d) **	1 -15000	-	-	510	1275	3795	7020	-	-	-	-	-	-
Tt (°C)	-2.5-2.5	-	-	-	-	-	-	-0.94-2.08	-0.88-1.75	-2.15-1.57	-1.84-1.81	-1.74-0.16	-1.92-1.54
C_{melt} ($mm^oC^{-1}d^{-1}$)	1-5	-	-	-	-	-	-	2.32-4.42	1.67-3.96	1.79-3.77	2.30-4.89	1.56-3.25	1.23-4.10
S_{imaxF} (mm)	0.1-5	-	-	-	-	-	-	1.53-3.73	1.35-4.39	0.55-4.10	3.18-4.03	2.94-4.98	2.04-4.39
S_{imaxG} (mm)	0.1-5	-	-	-	-	-	-	-	-	-	0.30-0.60	0.46-0.70	0.38-1.39
C_a (-)	0.1-0.7	-	-	-	-	-	-	0.24-0.43	0.35-0.55	0.33-0.62	0.30-0.66	0.38-0.52	0.30-0.56
S_{umaxF} (mm)	50-500	-	-	-	-	-	-	314-415	236-355	233-464	355-438	301-441	352-485
S_{umaxG} (mm)	50-500	-	-	-	-	-	-	-	-	-	161-199	152-287	173-297
S_{umaxW} (mm)	50-500	-	-	-	-	-	-	-	-	-	56-149	89-149	85-148
γ_F (-)	0.1-5	-	-	-	-	-	-	0.93-1.68	0.61-1.01	0.57-2.03	0.99-4.59	2.04-3.98	0.76-4.94
γ_G (-)	0.1-5	-	-	-	-	-	-	-	-	-	0.15-0.26	0.23-0.53	0.11-0.52
γ_W (-)	0.1-5	-	-	-	-	-	-	-	-	-	0.14-3.64	0.12-0.32	0.10-2.88
D (-)	0-1	-	-	-	-	-	-	0.30-0.77	0.41-0.81	0.30-0.69	0.03-0.35	0.06-0.33	0.03-0.33
C_{pmaxF} (mm d^{-1})	0.1-4	-	-	-	-	-	-	1.04-2.03	0.98-1.83	1.05-2.62	0.91-3.19	0.94-3.66	1.37-3.72
C_{pmaxG} (mm d^{-1})	0.1-4	-	-	-	-	-	-	-	-	-	0.74-1.80	0.22-1.17	0.93-2.13
C_{rmax} (mm d^{-1})	0-4	-	-	-	-	-	-	-	-	-	0.00-0.31	0.02-1.06	0.01-0.98
K_{fF} (d^{-1})	0.2-5	-	-	-	-	-	-	0.27-2.99	0.24-1.52	0.31-3.79	0.21-3.03	0.21-0.70	0.50-4.21
K_{fG} (d^{-1})	0.2-5	-	-	-	-	-	-	-	-	-	0.21-4.04	0.25-0.41	0.25-3.66
Ks (d^{-1})	0.002-0.2	-	-	-	-	-	-	0.04-0.19	0.05-0.18	0.05-0.18	0.05-0.17	0.03-0.14	0.05-0.17
$S_{s,p}$ (mm)	100-20000	-	-	-	-	-	-	4107-10029	3924-9339	4078-13676	4278-9011	3270-4622	4150-8568

Table 4. Performance metrics of the model implementations and the associated calibration strategies for the 2001 – 2009 calibration period (cal.) and the 2010 – 2016 model evaluation period (val.). For brevity only the values for the most balanced solution, i.e., lowest D_E (Eq. 14) are shown here. The ranges of all performance metrics for the full set of pareto optimal solutions for the multi-objective calibration cases (Scenarios 7 – 12) are provided in the Table S5 in supplement. *) The MSE values provided for C_x describe the sine wave fits of both, the precipitation and stream flow $\delta^{18}O$ signals, respectively.

Scenario			1	2	3	4	5	6	7	8	9	10	11	12
Model			SW-EM	SW-GM	CO-EM		CO-GM		IM-SAS-L			IM-SAS-D		
Implementation			Lumped									Distributed		
Calibration strategy → Performance metric ↓			C_x	C_x	$C_{\delta^{18}O}$	C^3_H	$C_{\delta^{18}O}$	C^3_H	$C_{\delta^{18}O,Q}$	$C^3_{H,Q}$	$C_{\delta^{18}O,^3H,Q}$	$C_{\delta^{18}O,Q}$	$C^3_{H,Q}$	$C_{\delta^{18}O,^3H,Q}$
Performance metrics	$MSE_{\delta^{18}O}$	cal.	3.850/0.121*)		0.334	-	0.213	-	0.083	-	0.118	0.079	-	0.114
		val.	5.208/0.144*)		0.430	-	0.245	-	0.332	-	0.273	0.273	-	0.275
	$MSE_{^3H}$	cal.	-	-	-	5.904	-	5.810	-	2.972	2.823	-	2.920	2.981
		val.	-	-	-	5.160	-	4.468	-	2.389	2.285	-	2.357	2.450
	MSE_Q	cal.	-	-	-	-	-	-	0.202	0.299	0.308	0.228	0.263	0.317
		val.	-	-	-	-	-	-	0.224	0.297	0.329	0.251	0.283	0.336
	$MSE_{log(Q)}$	cal.	-	-	-	-	-	-	0.120	0.158	0.174	0.130	0.171	0.161
		val.	-	-	-	-	-	-	0.120	0.148	0.150	0.127	0.201	0.165
	MSE_{FDC_Q}	cal.	-	-	-	-	-	-	0.058	0.024	0.073	0.022	0.017	0.025
		val.	-	-	-	-	-	-	0.103	0.022	0.142	0.043	0.065	0.059
	$MSE_{FDC_{log(Q)}}$	cal.	-	-	-	-	-	-	0.011	0.011	0.047	0.006	0.019	0.009
		val.	-	-	-	-	-	-	0.015	0.009	0.047	0.009	0.050	0.018
	MSE_{RC}	cal.	-	-	-	-	-	-	0.004	0.005	0.007	0.003	0.006	0.003
		val.	-	-	-	-	-	-	0.004	0.004	0.005	0.003	0.008	0.003
	MSE_{AC_Q}	cal.	-	-	-	-	-	-	0.003	0.002	0.003	0.002	0.001	0.001
		val.	-	-	-	-	-	-	0.008	0.002	0.001	0.005	0.002	0.007

https://doi.org/10.5194/hess-2022-400
Preprint. Discussion started: 13 December 2022

Hydrology and Earth System Sciences
Discussions

1040

Table 5. Metrics of stream flow TTDs derived from the 12 model scenarios with the different associated calibration strategies, where $C_{\delta^{18}O}$ indicates calibration to $\delta^{18}O$, C^{3}_{H} calibration to ^{3}H, while $C_{\delta^{18}O,Q}$, $C^{3}_{H,Q}$ and $C_{\delta^{18}O,^{3}H,Q}$ indicate multi-objective, i.e. simultaneous calibration to combinations of $\delta^{18}O$, ^{3}H and stream flow. The TTD metrics for scenarios 1-6 represent the best fits of the respective time-invariant TTD, while for scenarios 7-12 the mean and standard deviations of all daily streamflow TTDs during the modelling period 01/10/2001 – 31/12/2016 are given. The mean transit time for scenarios 7 – 12 was estimated by fitting Gamma distributions to the volume-weighted mean TTDs of each individual scenario. The water fractions are shown as the fractions of below a specific age T. The columns with absolute difference Δ illustrate the differences in TTDs from the same models calibrated to $\delta^{18}O$ and ^{3}H, respectively. The subscripts indicate the scenarios that are compared (e.g., $\Delta_{3,4}$ compares scenarios 3 and 4). *Note that the fraction of water younger than 3 months is comparable to the fraction of young water as suggested by Kirchner (2016).

	Scenario	1	2	3	4	5	6	7	8	9	10	11	12	$\Delta_{3,4}$	$\Delta_{5,6}$	$\Delta_{7,8}$	$\Delta_{10,11}$
	Model	SW-EM	SW-GM	CO-EM		CO-GM		IM-SAS-L			IM-SAS-D			Absolute difference			
	Calibration strategy → TTD metrics ↓	C_x	C_x	$C_{\delta^{18}O}$	C^{3}_{H}	$C_{\delta^{18}O}$	C^{3}_{H}	$C_{\delta^{18}O,Q}$	$C^{3}_{H,Q}$	$C_{\delta^{18}O,^{3}H,Q}$	$C_{\delta^{18}O,Q}$	$C^{3}_{H,Q}$	$C_{\delta^{18}O,^{3}H,Q}$	$\Delta TT_{\delta^{18}O-^{3}H}$ $\Delta F(T<x)_{\delta^{18}O-^{3}H}$			
Percentiles (yr)	Mean (yr)	0.7	1.8	1.4	10.4	1.7	9.6	18.2	14.1	13.6	16.0	15.0	14.0	-9.0	-7.9	4.1	1.0
	10^{th}	0.1	< 0.1	0.1	1.1	< 0.1	0.2	0.5±0.7	0.5±0.8	0.4±0.6	0.3±0.5	0.3±0.5	0.3±0.4	-1.0	-0.2	0.0	0.0
	25^{th}	0.2	0.2	0.4	3.0	0.2	1.0	2.1±2.1	1.9±2.1	1.5±1.8	2.1±1.7	1.5±1.7	1.4±1.5	-2.6	-0.8	0.2	0.6
	50^{th} (median)	0.5	0.8	1.0	7.2	0.8	4.4	9.0±3.3	6.5±4.8	5.7±4.3	8.6±2.6	6.7±3.7	6.6±3.5	-6.2	-3.6	2.5	1.9
	75^{th}	1.0	2.3	1.9	14.4	2.3	12.7	22.2±3.3	17.6±6.5	16.3±6.2	20.8±2.8	18.8±4.6	17.8±4.2	-12.5	-10.4	4.6	2.0
	90^{th}	1.7	4.8	3.2	23.9	4.7	25.9	31.3±4.3	29.2±5.0	28.6±5.1	31.1±4.2	30.4±4.3	29.9±4.2	-20.7	-21.2	2.1	0.7
Water fractions (%)	F(T<3 m)*	29	29	16	2	29	12	18±12	23±19	21±15	16±10	22±13	23±15	14	17	-5	-6
	F(T<6 m)	49	41	30	5	41	18	21±13	29±22	30±19	20±11	27±16	27±16	25	23	-8	-7
	F(T<1 yr)	74	55	51	9	55	25	24±13	32±22	35±21	22±11	30±16	29±15	41	30	-8	-8
	F(T<3 yr)	98	81	88	25	81	42	31±11	39±20	42±19	30±10	37±14	37±14	63	39	-8	-7
	F(T<5 yr)	100	91	97	38	91	53	38±10	46±18	49±17	38±9	44±13	44±12	59	38	-8	-6
	F(T<10 yr)	100	98	100	62	98	69	52±8	59±13	62±12	53±7	58±10	58±9	38	29	-7	-5
	F(T<20 yr)	100	100	100	85	100	85	71±5	77±7	79±7	74±4	76±5	77±5	15	15	-6	-2

1055

https://doi.org/10.5194/hess-2022-400
Preprint. Discussion started: 13 December 2022

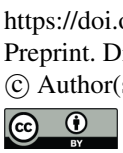

Hydrology and Earth System Sciences
Discussions
Open Access
EGU

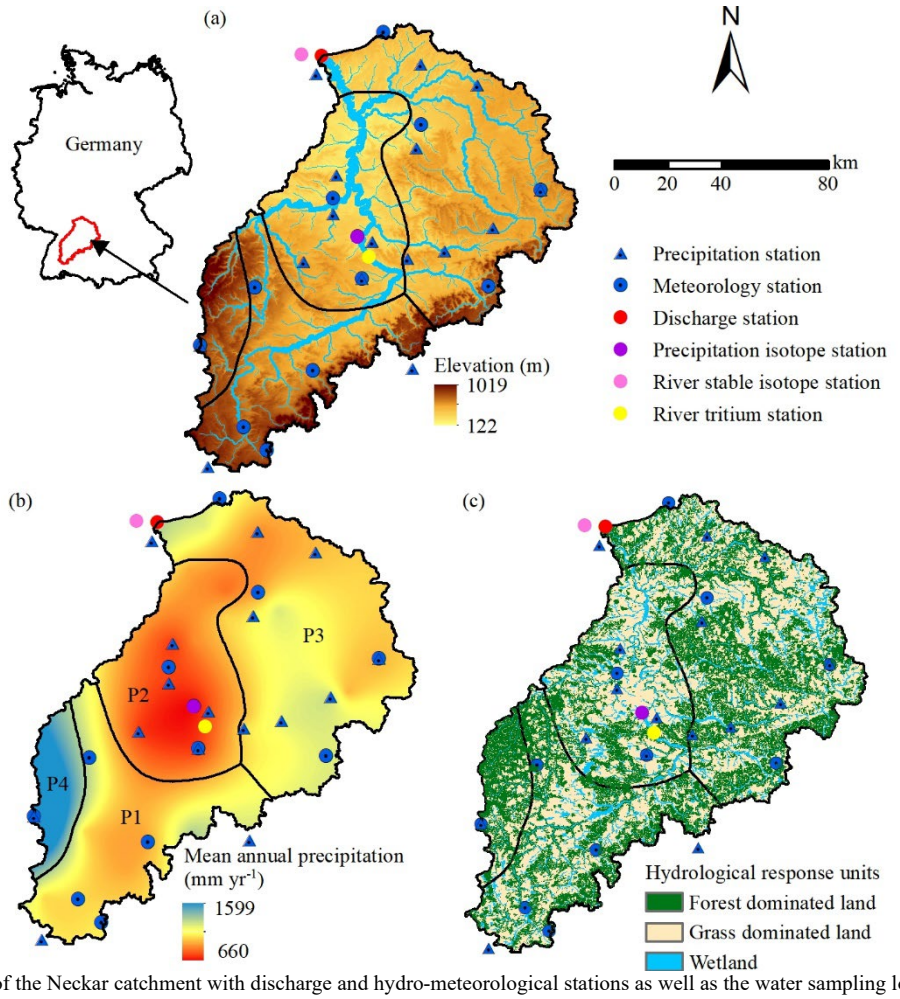

1060 **Figure 1.** (a) Elevation of the Neckar catchment with discharge and hydro-meteorological stations as well as the water sampling locations used in this study, (b) the spatial distribution of long-term mean annual precipitation in the Neckar catchment and the stratification into four distinct precipitation zones P1 – P4, (c) hydrological response units classified according to their land-cover and topographic characteristics.

https://doi.org/10.5194/hess-2022-400
Preprint. Discussion started: 13 December 2022

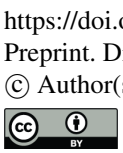

Hydrology and Earth System Sciences
Discussions
Open Access
EGU

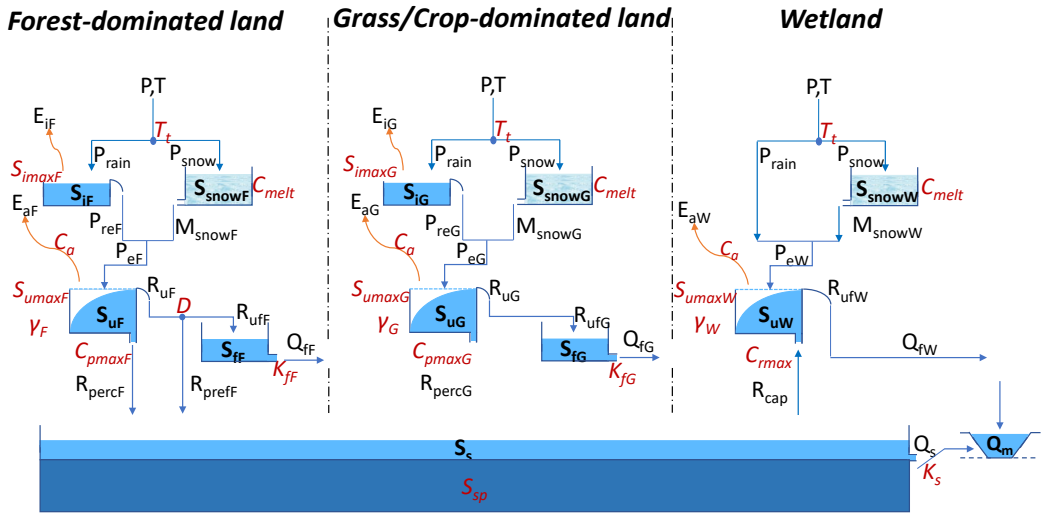

1065 **Figure 2.** Model structure of the integrated model, discretized into three parallel hydrological response units HRU, i.e. forest, grassland and wetland in each precipitation zone P1 – P4. The light blue boxes indicate the hydrologically active individual storage volumes. The dark blue box indicates the hydrologically passive storage volume $S_{s,p}$. The arrow lines indicate water fluxes and model parameters are shown in red. All symbols are described in Table S4 in the Supplementary Material.

https://doi.org/10.5194/hess-2022-400
Preprint. Discussion started: 13 December 2022

Hydrology and Earth System Sciences
Discussions
Open Access
EGU

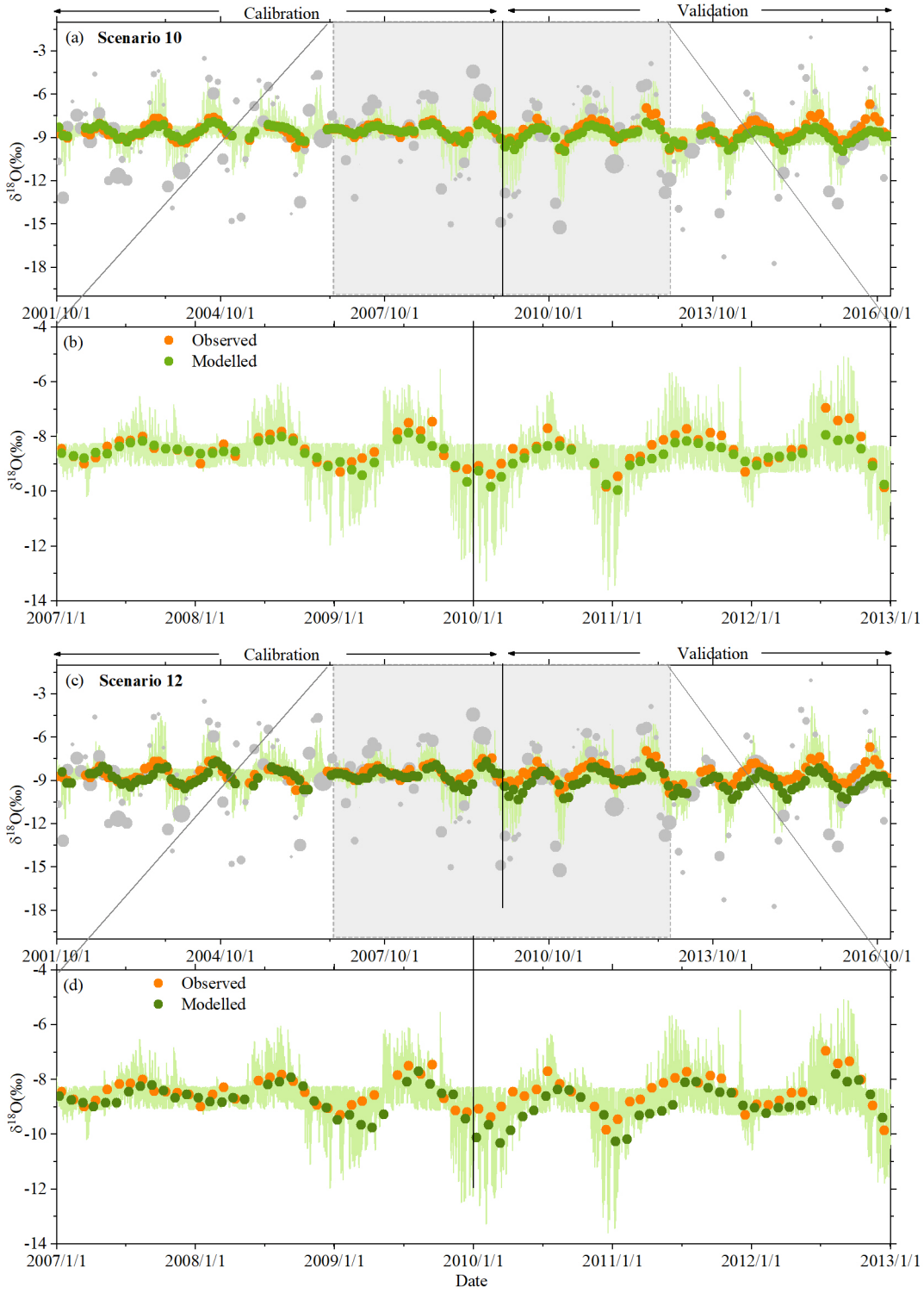

1070 **Figure 3**. The time series of stream $\delta^{18}O$ reproduced by model IM-SAS-D based on simultaneous calibration to $\delta^{18}O$ and the streamflow signatures, i.e. calibration strategy $C_{\delta^{18}O,Q}$ (scenario 10) and $C_{\delta^{18}O,^3H,Q}$ (scenario 12), for the model calibration and evaluation periods. (a) Observed $\delta^{18}O$signals in precipitation

https://doi.org/10.5194/hess-2022-400
Preprint. Discussion started: 13 December 2022

Hydrology and Earth System Sciences
Discussions

(light grey dots; size of dots indicates the precipitation volume) and observed stream $\delta^{18}O$ signals (orange dots) as well as the most balanced, i.e. lowest D_E, modelled $\delta^{18}O$ signal in the stream (green dots) for scenario 10 and the $5^{th}/95^{th}$ percentile of all retained pareto optimal solutions obtained from calibration strategy $C_{\delta^{18}O,Q}$ (green shaded area), (b) zoom-in of observed and modelled $\delta^{18}O$ signals in the stream for the 01/01/2007 – 31/12/2012 period for scenario 10,
1075 (c) Observed $\delta^{18}O$signals in precipitation and in stream same as (a), and the modelled stream $\delta^{18}O$signals (relatively darker green dots) for scenario 12 and the $5^{th}/95^{th}$ percentile of all retained pareto optimal solutions obtained from calibration strategy $C_{\delta^{18}O,^3H,Q}$ (light green shaded area), (d) zoom-in of observed and modelled $\delta^{18}O$ signals in the stream for the 01/01/2007 – 31/12/2012 period for scenario 12.

https://doi.org/10.5194/hess-2022-400
Preprint. Discussion started: 13 December 2022

Hydrology and Earth System Sciences
Discussions
Open Access
EGU

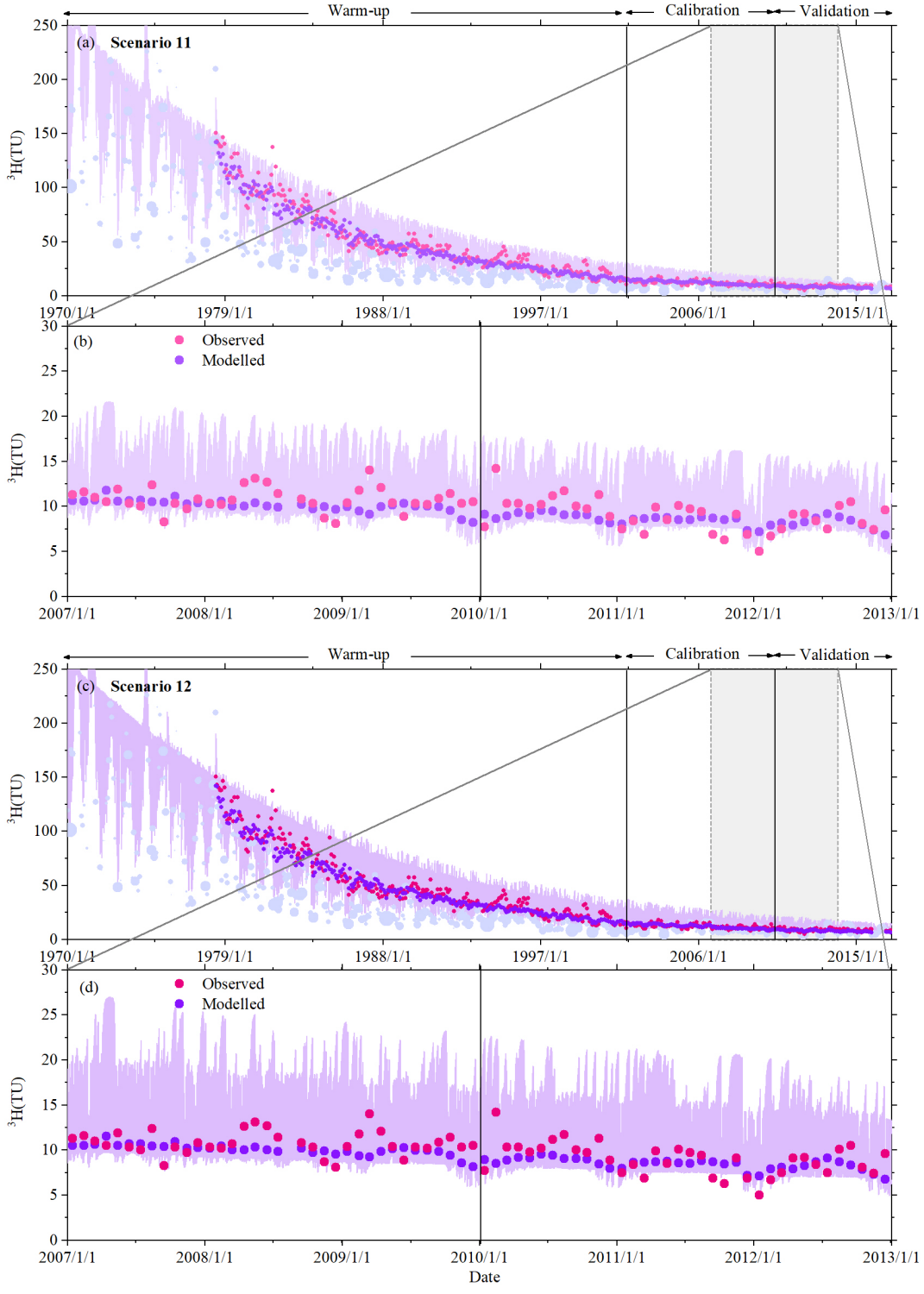

Figure 4. Time series of stream ^{3}H reproduced by model IM-SAS-D based on simultaneous calibration to ^{3}H and the streamflow signatures, i.e. calibration strategy $C_{^3H,Q}$ (scenario 11) and $C_{\delta^{18}O,^3H,Q}$ (scenario 12), for the model calibration and evaluation periods. (a) Observed ^{3}H signals in precipitation (light blue-

https://doi.org/10.5194/hess-2022-400
Preprint. Discussion started: 13 December 2022

Hydrology and Earth System Sciences
Discussions

purple dots; size of dots indicates associated precipitation volume) and in streamflow (pink dots) as well as the modelled ^{3}H stream signal based on the most balanced solution, i.e. lowest DE (purple dots), and the 5th/95th inter-quantile range of all retained pareto optimal solutions obtained from calibration strategy $C^{3}_{H,Q}$ (purple shaded area) for scenario 11, (b) zoom-in of observed and modelled ^{3}H signals for the 01/01/2007 – 31/12/2012 period for scenario 11, (c) Observed ^{3}H signals in precipitation and in stream same as (a), and the modelled stream ^{3}H signals (relatively darker purple dots) for scenario 12 and the 5th/95th percentile of all retained pareto optimal solutions obtained from calibration strategy $C_{\delta^{18}O,^{3}H,Q}$ (light purple shaded area), (d) zoom-in of observed and modelled ^{3}H signals in the stream for the 01/01/2007 – 31/12/2012 period for scenario 12.

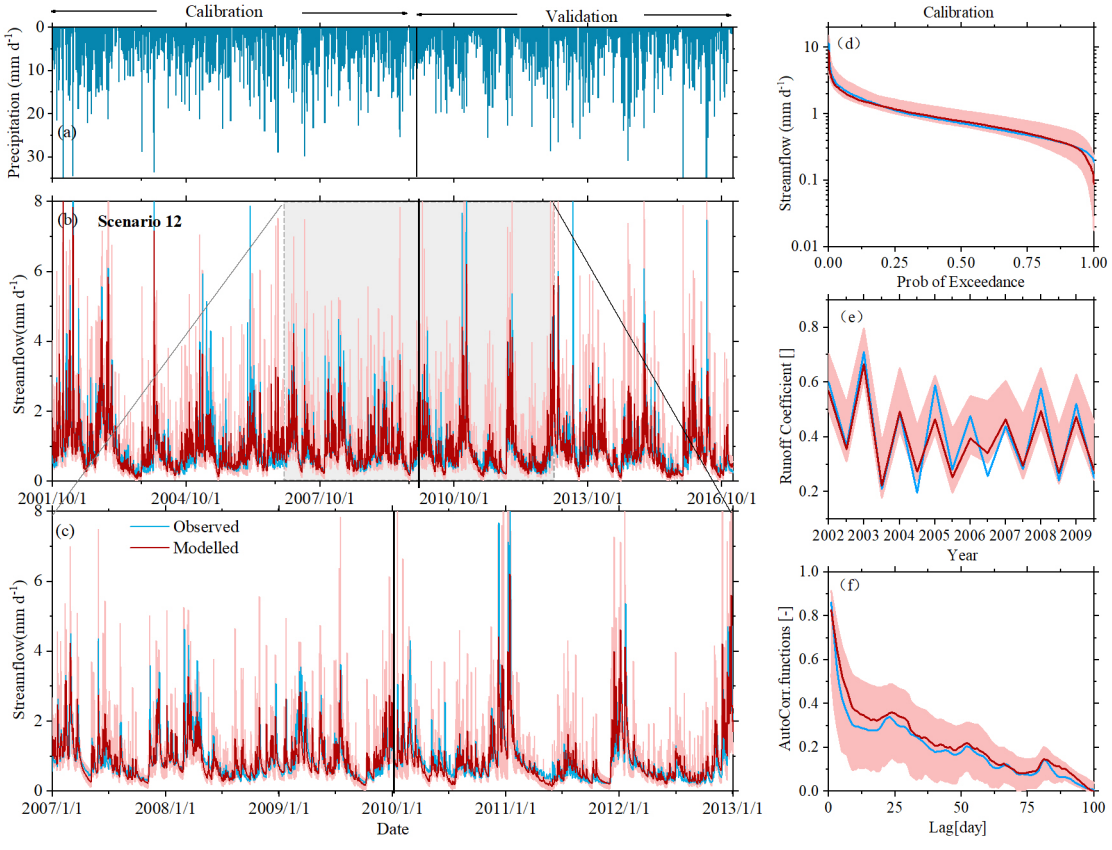

Figure 5. Hydrograph and selected hydrological signatures reproduced by IM-SAS-D, following a simultaneous calibration to the hydrological response, $\delta^{18}O$ and ^{3}H ($C_{\delta^{18}O,^{3}H,Q}$; scenario 12). (a) Time series of observed daily precipitation; observed and modelled (b) daily stream flow (Q), where the red line indicates the most balanced solution, i.e., lowest D_E, and the red shaded area the 5th/95th inter-quantile range obtained from all pareto optimal solutions; (c) stream flow zoomed-in to the 01/01/2007 – 31/12/2012 period; (d) flow duration curves (FDC_Q), (e) seasonal runoff coefficients (RC_Q) and (f) autocorrelation functions of stream flow (AC_Q) for the calibration period. Blue lines indicate values based on observed streamflow (Q_o), red lines are values based on modelled stream flow (Q_m) representing the most balanced solutions, i.e., lowest D_E and the red shaded areas show the 5th/95th inter-quantile ranges obtained from all pareto optimal solutions.

https://doi.org/10.5194/hess-2022-400
Preprint. Discussion started: 13 December 2022

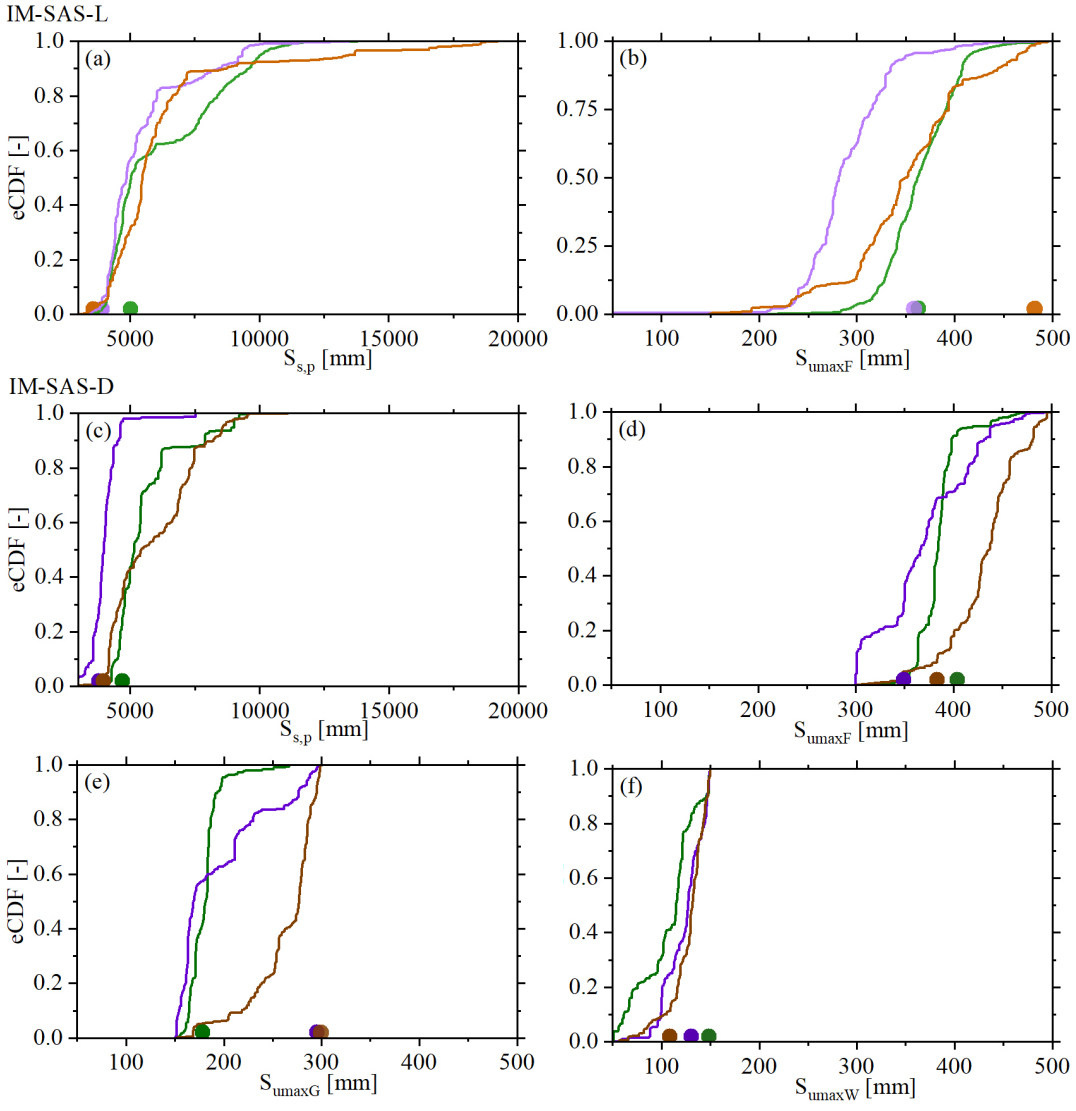

Figure 6 Pareto-optimal distributions of selected parameters of the IM-SAS models (i.e., IM-SAS-L, IM-SAS-D) shown as the associated empirical cumulative distribution functions (lines). Light green shades indicate scenario 7, light purple shades indicate scenario 8 and light brown shades indicate scenario 9 in (a) and (b); relatively darker green shades indicate scenario 10, relatively darker purple shades indicate scenario 11 and relatively darker brown shades indicate scenario 12 in (c) - (f). The dots indicate the parameter values associated with the most balanced solution, i.e., lowest D_E.

https://doi.org/10.5194/hess-2022-400
Preprint. Discussion started: 13 December 2022

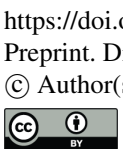

Hydrology and Earth System Sciences
Discussions

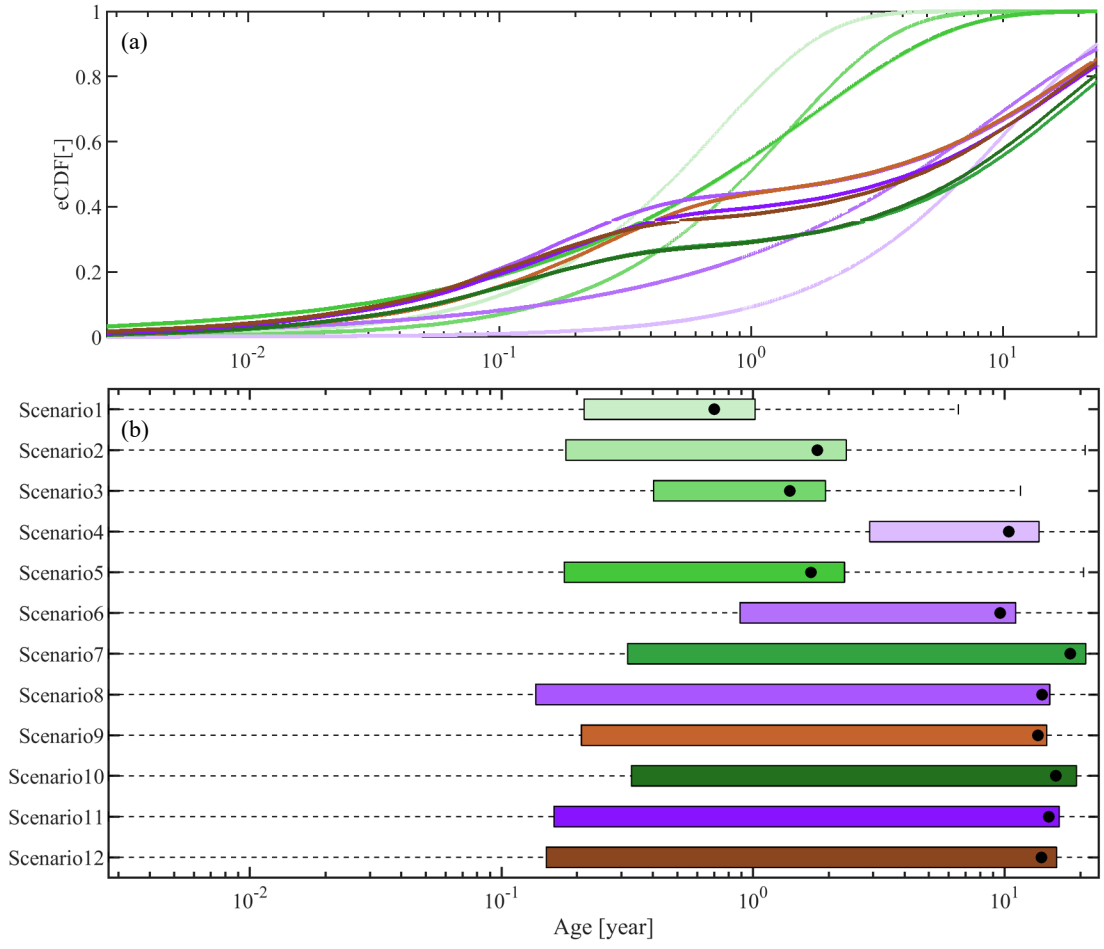

Figure 7. Stream flow TTDs derived from the 12 model scenarios with the different associated calibration strategies. The TTDs for scenarios 1-6 represent the best fits of the respective time-invariant TTD, while for scenarios 7-12 the volume weighted average daily TTDs during the modelling period 01/10/2001 – 31/12/2016 are given. Green shades represent the TTDs inferred from $\delta^{18}O$ based on different models (from lighter to darker for scenarios 1, 2, 3, 5, 7 and 10) in (a) and (b); the purple shades represent TTDs inferred from ^{3}H based on different models (from lighter to darker for scenario 4, 6, 8, 11), the brown lines represent TTDs inferred from combined $\delta^{18}O$ and ^{3}H based on different models (brown shades from lighter to darker for scenario 9 and 12); the black dots in (b) indicate the mean transit time for each of 12 model scenarios. Note that the mean transit time for scenarios 7 – 12 was estimated by fitting Gamma distributions to the volume-weighted mean TTDs of each individual scenario.

https://doi.org/10.5194/hess-2022-400
Preprint. Discussion started: 13 December 2022

Hydrology and Earth System Sciences
Discussions
Open Access
EGU

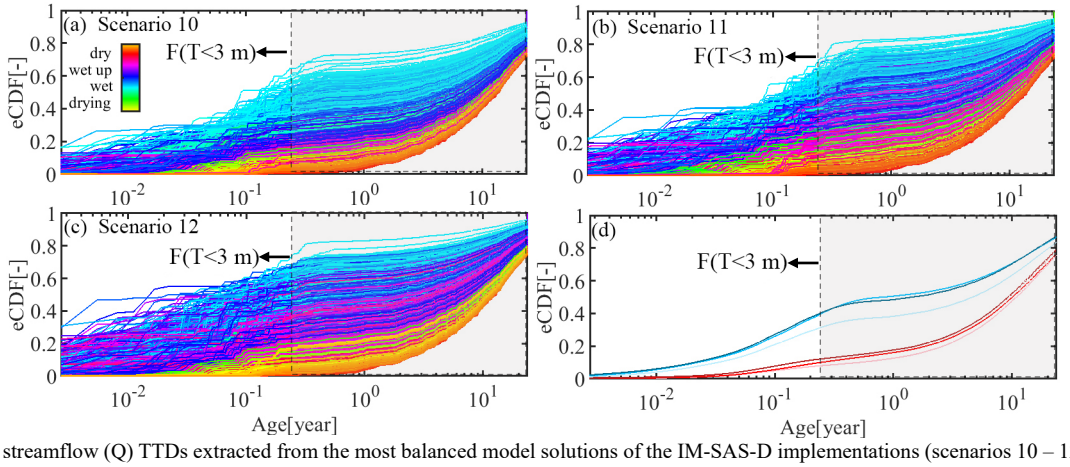

Figure 8. Daily streamflow (Q) TTDs extracted from the most balanced model solutions of the IM-SAS-D implementations (scenarios 10 – 12), based on (a) calibration strategy $C_{\delta^{18}O,Q}$ (scenario 10), (b) calibration strategy $C^{3}_{H,Q}$ (scenario 11) and (c) calibration strategy $C_{\delta^{18}O,^{3}H,Q}$ (scenario 12). The line colors represent the transition between dry and wet periods. Panel (d) shows the volume weighted average TTDs for the wet and dry periods, respectively. The light shades represent calibration strategy $C_{\delta^{18}O,Q}$ (scenario 10), the intermediate shades indicate calibration strategy $C^{3}_{H,Q}$ (scenario 11) and the dark shades are calibration strategy $C_{\delta^{18}O,^{3}H,Q}$ (scenario 12). For illustrative purposes, also the fraction of water younger than 3 months F (T < 3 m) is indicated.

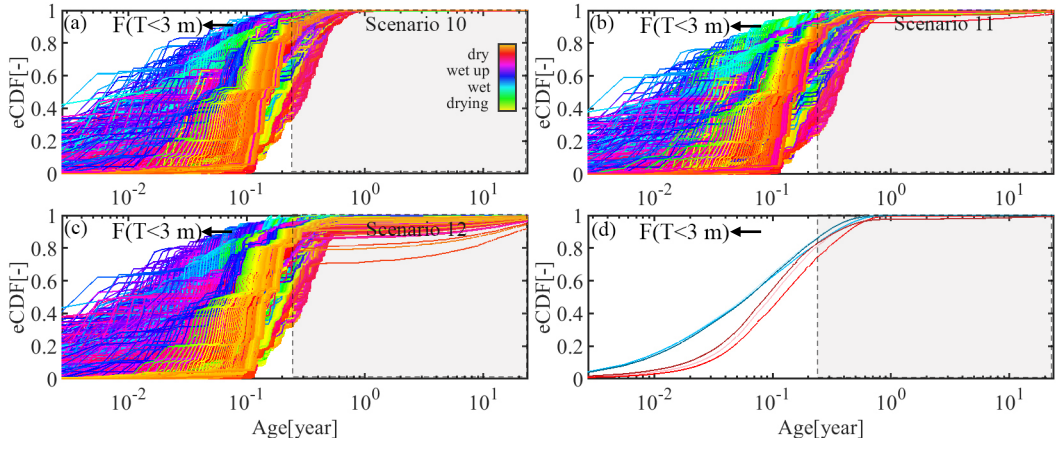

Figure 9. Daily transpiration (E_a) TTDs extracted from the most balanced model solutions of the IM-SAS-D implementations (scenarios 10 – 12), based on (a) calibration strategy $C_{\delta^{18}O,Q}$ (scenario 10), (b) calibration strategy $C^{3}_{H,Q}$ (scenario 11) and (c) calibration strategy $C_{\delta^{18}O,^{3}H,Q}$ (scenario 12). The line colors represent the transition between dry and wet periods. Panel (d) shows the volume weighted average TTDs for the wet and dry periods, respectively. The light shades represent calibration strategy $C_{\delta^{18}O,Q}$ (scenario 10), the intermediate shades indicate calibration strategy $C^{3}_{H,Q}$ (scenario 11) and the dark shades are calibration strategy $C_{\delta^{18}O,^{3}H,Q}$ (scenario 12). For illustrative purposes, also the fraction of water younger than 3 months F (T < 3 m) is indicated.

https://doi.org/10.5194/hess-2022-400
Preprint. Discussion started: 13 December 2022

Hydrology and Earth System Sciences
Discussions
Open Access
EGU

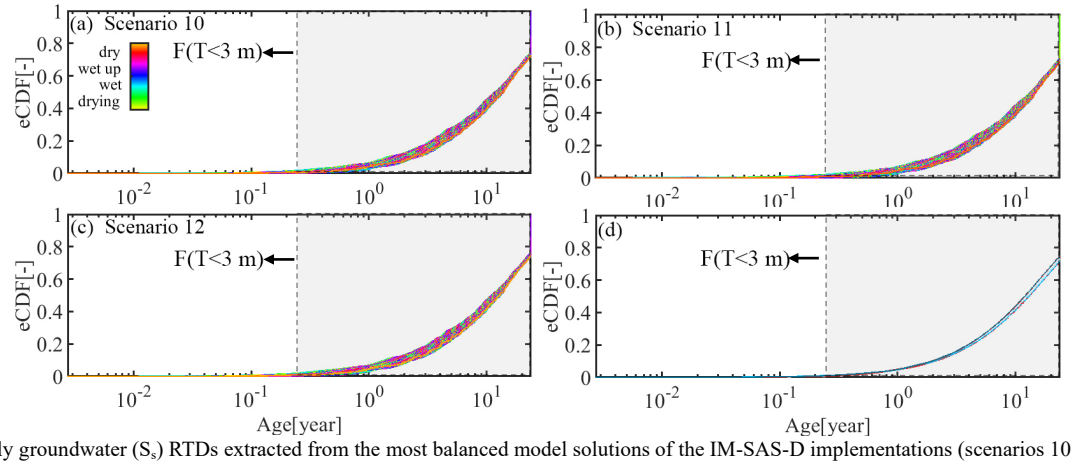

Figure 10. Daily groundwater (S_s) RTDs extracted from the most balanced model solutions of the IM-SAS-D implementations (scenarios 10 – 12), based on (a) calibration strategy $C_{\delta^{18}O,Q}$ (scenario 10), (b) calibration strategy $C^{3}_{H,Q}$ (scenario 11) and (c) calibration strategy $C_{\delta^{18}O,^{3}H,Q}$ (scenario 12). The line colors represent the transition between dry and wet periods. Panel (d) shows the volume weighted average RTDs for the wet and dry periods, respectively. The light shades represent calibration strategy $C_{\delta^{18}O,Q}$ (scenario 10), the intermediate shades indicate calibration strategy $C^{3}_{H,Q}$ (scenario 11) and the dark shades are calibration strategy $C_{\delta^{18}O,^{3}H,Q}$ (scenario 12). For illustrative purposes, also the fraction of water younger than 3 months F (T < 3 m) is indicated.